Title: Transcriptome network analysis of human CD1c+ dendritic cells identifies an inflammatory cytokine-secreting subpopulation within the CD14+ DC3s that accumulates locally in type I IFN-negative autoimmunity to the eye

Authors:

S. Hiddingh[1,3†], A. Pandit[3,4†], F.H. Verhagen[1-3†], R. Rijken[3,4], N. H. Servaas[3,4], C.G.K. Wichers[3,4], N.H. ten Dam-van Loon[2], S.M. Imhof[1,2], T.R.D.J. Radstake[5‡], J.H. de Boer[1,2‡], J.J.W. Kuiper[1-3‡*]

Affiliations:

[1] Ophthalmo-Immunology, University Medical Center Utrecht, Utrecht University, Utrecht, the Netherlands.

[2] Department of Ophthalmology, University Medical Center Utrecht, Utrecht University, Utrecht, the Netherlands.

[3] Center for Translational Immunology, University Medical Center Utrecht, Utrecht University, Utrecht, the Netherlands.

[4] Department of Rheumatology & Clinical Immunology, University Medical Center Utrecht, Utrecht University, Utrecht, the Netherlands.

[5] University Medical Center Utrecht and Utrecht University, Utrecht, The Netherlands and AbbVie, Chicago, IL.

[*] these authors contributed equally,

[†] these authors contributed equally.

* Corresponding author:

J.J.W. Kuiper J.J.W.Kuiper@umcutrecht.nl Heidelberglaan 100, 3584CX, Utrecht, The Netherlands.

ABSTRACT

Background: Inflammatory subsets of CD1c+ conventional dendritic cells (CD1c+ DCs) are promoted by type I interferons (IFN), but the molecular basis for CD1c+ DCs involvement in conditions not driven by type I IFNs is unknown.

Methods: Our objective was to use RNA-sequencing of blood CD1c+ DCs and high-dimensional flow cytometry of two cohorts of non-infectious uveitis patients and healthy donors to characterize the CD1c+ DCs population of type I IFN-*negative* autoimmunity.

Results: We report that the CD1c+ DCs pool from patients with non-infectious uveitis (n=42) is skewed towards a transcriptional network characterized by surface receptor genes *CX3CR1, CCR2,* and *CD36,* but not *CD14*. We confirmed these results by RNA-sequencing in another case-control cohort (n=36) and show that this gene network is controlled by NOTCH2-RUNX3 signaling, but is not conditional on CD14 surface expression. Unbiased flow cytometry analysis based on the transcriptional network identified a CD36+CX3CR1+ subpopulation within the CD14+ DC3 subset that was diminished in peripheral blood of patients. CD36+CX3CR1+ DC3s infiltrate eyes of patients and displayed a distinctive ability to produce high levels of inflammatory cytokines, including TNF-alpha, and IL-6, but not IL-23.

Conclusions: These results show that CD36+CX3CR1+ CD1c+ DCs are a subpopulation of inflammatory CD14+ DC3s implicated in type I IFN-negative human non-infectious uveitis that secrete proinflammatory mediators that drive its pathophysiology.

Funding: The presented work is supported by UitZicht (project number #2014-4, #2019-10, an #2021-4). The funders had no role in the design, execution, interpretation, or writing of the study.

INTRODUCTION:

Non-infectious uveitis refers to a family of severe inflammatory eye conditions that are a leading cause of preventable vision loss in the Western world (*1,2*). The disease mechanism of non-infectious uveitis is poorly understood. T cells are considered to play a role in non-infectious uveitis predominantly based on a large body of mechanistic studies using *experimental autoimmune uveitis* (EAU) in rodents (*3,4*). In human non-infectious uveitis it is unknown where and through which signals these T cells are activated. Genetic studies of archetypal forms of non-infectious uveitis HLA-B27-associated anterior uveitis, and HLA-A29-associated Birdshot Uveitis, demonstrated strong genetic association with *HLA* and *ERAP* genes, indicating that antigen presentation is central to the etiology of non-infectious uveitis (*5-8*). Although the role of antigen presenting cells in non-infectious uveitis is under explored, dendritic cells – key antigen presenting cells - strongly promote EAU (*9-11*). Previous studies have shown that in blood, the proportion of CD1c+ conventional dendritic cells (CD1c+ DCs) is associated with disease activity (*12-14*), and dendritic cells increase in abundance in eye fluid of patients (*15*). Thus, it is important to understand the role of dendritic cells in non-infectious uveitis.

Recent single-cell studies have revealed that the human CD1c+ DC pool (and the murine equivalent termed "cDC2s") constitute at least two phenotypically distinct subsets that originate from distinct progenitors (*16-18*). Cytokines of the type I Interferon (IFN) family have been shown to promote the expansion of a discrete subset within the CD1c+ DC pool in peripheral blood, termed "DC3" (*16,19,20*), which increase in frequency in blood during the type I IFN-driven condition *systemic lupus erythematosus* (SLE)(*17*). However, in contrast to SLE, uveitis disease activity in humans is accompanied by decreased type I IFN levels (*21*). More importantly, while the administration of type I Interferons can induce *lupus-like* disease, type I interferon therapy suppresses non-infectious uveitis (*21-23*), suggesting a distinct disease mechanism for CD1c+ DC involvement in human non-infectious uveitis. Therefore, our understanding of the CD1c+ DC characteristics during autoimmunity is incomplete, especially for conditions not driven by type I IFNs.

Our objective was to use whole transcriptome profiling by bulk RNA-sequencing of peripheral blood CD1c+ DCs and multiparameter flow cytometry of two cohorts of non-infectious uveitis patients and healthy donors to characterize the core transcriptional features and subset composition of CD1c+ DCs in autoimmunity of the eye. We constructed data-driven co-expression networks that identified a *bona fide* CD1c+ DC transcriptional module in patients that helped identify a cytokine-producing inflammatory CD1c+ DC subset that diminishes from peripheral blood and infiltrates the inflamed eye in non-infectious uveitis.

MATERIAL AND METHODS

Patients and patient material

This study was conducted in compliance with the Helsinki principles. Ethical approval was requested and obtained from the Medical Ethical Research Committee in Utrecht (METC protocol number #14-065/M). All patients signed written informed consent before participation. We collected blood from a discovery cohort of 29 and a replication cohort of 22 adult patients (**Table 1**) with HLA-B27-associated Acute Anterior Uveitis (AU), Idiopathic Intermediate Uveitis (IU), or HLA-A29-associated Birdshot Uveitis (BU). Patients were recruited at the outbound patient clinic of the department of Ophthalmology of the University Medical Center Utrecht between July 2014 and January 2017. To minimize bias, we recruited twenty-nine age and sex matched anonymous blood donors of European Ancestry with no history of ocular inflammatory disease at the same institute to serve as unaffected controls (14 for the discovery cohort and 13 for the replication cohort). Uveitis was classified and graded in accordance with the SUN classification (*24*). Each patient underwent a full ophthalmological examination by an ophthalmologist experienced in uveitis, routine laboratory screening, and an X-Ray of the lungs. Laboratory screening included erythrocyte sedimentation rate, renal and liver function tests, angiotensin converting enzyme (ACE), and screening for infectious agents in the serum and an Interferon-Gamma Release Assay (IGRA) was obtained for all patients. All patients with AU and BU were HLA-B27 or HLA-A29-positive, respectively (confirmed by HLA typing). All patients had active uveitis (new onset or relapse) and there was no clinical evidence for

uveitis-associated systemic inflammatory disease (e.g., rheumatic condition) till the time of sampling. None of the patients received systemic immunomodulatory treatment in the last 3 months, other than low dose (≤10mg) oral prednisolone in one BU patient of the discovery cohort and one AU patient of the replication cohort.

CD1c+ DC purification

Peripheral blood mononuclear cells (PBMCs) were isolated by standard ficoll density gradient centrifugation from 70mL heparinized blood immediately after blood withdrawal (GE Healthcare, Uppsala, Sweden). For the discovery cohort, fresh PBMCs were immediately subjected to magnetic-activated cell sorting (MACS) for the removal (positive selection) of CD304+ cells (pDC), followed by CD19+ cells (B cell), and subsequently isolation of CD1c+ cells by using the CD1c+ (BDCA1) isolation kit (Miltenyi Biotec, Germany) according to the manufacturer's instructions. The isolated CD1c+ fraction contained on average 147,114 cells (range 46,000-773,000) and purity was determined by flow cytometry measured on the BD LSR Fortessa™ Cell analyzer (**Supplementary File 1A**). Data were analyzed using FlowJo software (TreeStar Inc.). For the replication cohort, ten batches (individual days) of 4-5 randomly selected patient and control samples of nitrogen stored PBMCs (mean storage time of 11 [range 0-31] months) were carefully thawed and subjected to sorting by the BD FACSAria™ III sorter after incubation with a panel of surface antibodies (**Supplementary File 1B**) and FACS buffer (1% bovine serum albumin and 0.1% sodium azide in phosphate buffered saline). CD3-CD19-CD56-HLA-DR+CD11c+CD1c+CD14- cells were sorted. The average number of collected cells by sorting was 56,881 (range 6,669-243,385). MACS or FACS purified CD1c+ cells were immediately taken up in a lysis buffer (RLT plus, Qiagen) containing 1% β-mercaptoethanol, snap frozen on dry ice, and stored at -80°C until RNA extraction was performed. Isolation of CD1c+ DC for functional experiments was done by MACS as described above. Purification of CD1c+ DC subsets based on CD36 and CX3CR1 or CD14 expression from freshly isolated PBMCs was conducted by flow cytometry using the panel in **Supplementary File 1C** and shown in **Figure 5 – Supplement 1**.

CD1c+ DC cultures and secretome analysis.

Purified CD1c+ DCs were cultured in RPMI Glutamax (Thermo Fisher Scientific) supplemented with 10% heat-inactivated fetal bovine serum (FBS) (Biowest Riverside) and 1% penicillin/streptomycin (Thermo Fisher Scientific). CD1c+ DCs were cultured at a concentration of 0.5×10^6 cells/mL in a 96-well round-bottom plate (100µL/well). Cells were stimulated overnight (18 hours) with multiple stimuli listed in **Supplementary File 1D**. After stimulation, cells were lysed in an *RLT plus* lysis buffer (Qiagen) and stored at -80°C until RNA extraction was performed. Cell lysates were stored at -80°C until RNA extraction was performed for qPCR. In separate cultures, CD1c+ DC subsets (based on CD36 and CX3CR1 expression) were cultured in the presence of 1µg/mL Lipoteichoic acid (LTA). After 18 hours of stimulation, supernatants were harvested and IL-23 cytokine production was analyzed by ELISA (R&D Systems). The levels of IL-2, IL-5, IL-6, IL-10, IL-12p70, IL-13, IL-17, IL-22, IL-27, TNF-alpha, IFN-alpha, IFN-beta, CCL1, CXCL10, CXCL13, VEGF, CD40L, FAS, TNFR1, TNFR2, Elastase, and Granzyme B were simultaneously measured in supernatant of CD1c+ DC cultures using the in-house multiplex immunoassay based on Luminex technology, as described previously (*25*). Protein concentrations that were out of range were replaced with the LLOQ (lower limit of quantification) and ULOQ (upper limit of quantification) for each analyte and divided by 2 for the proteins detected below the range of detection or multiplied by 2 for values above the detection range (**Supplementary File 1E**).

Real-time Quantitative PCR

First-strand cDNA was synthesized from total RNA using Superscript IV kit (Thermo Fisher Scientific), and quantitative real-time PCR (RT-qPCR) was performed on the QuantStudio 12k flex System (LifeTechnologies), following manufacturer's instructions. Sequences of the primers used are listed in **Supplementary File 1F** and the *Key Resource Table***.** RT-qPCR data were normalized to the expression of the selected housekeeping gene *GUSB* (ENSG00000169919). CT values were normalized to *GUSB* by subtracting the CT mean of

GUSB (measured in duplo) from the CT mean of the target mRNA (i.e., *CD36*, *RUNX3)* = ΔCT. The fold change (FC) of each sample was calculated compared to ΔCt of the medium control using the formula FC = 2−ΔΔCt, where ΔΔCt = ΔCt sample—ΔCt reference.

Flow cytometry of CD1c+ DC populations

PBMC samples from the discovery and replication cohort (HC 11 samples; AU 9 samples; IU 6 samples; BS 11 samples) were randomly selected and measured by flow cytometry in batches of 9 to 10 mixed samples per run, divided over 4 days. Per batch, 10 million PBMCs per sample were quickly thawed, washed with ice cold PBS and stained with the antibody panel depicted in **Supplementary File 1C**. PBMCs were incubated with Fixable Viability Dye eF780 (eBioscience) at room temperature for 10 minutes. Cells were then plated in V-bottomed plates (Greiner Bio-one), washed with PBS and incubated for 30 minutes at 4˚C in the dark with Brilliant Stain Buffer (BD) and the fluorescently-conjugated antibodies. Next, the cells were washed and taken up in the FACS buffer. Flow cytometric analyses were performed on the BD FACSAria™ III sorter. Manual gating of data was done using FlowJo software (TreeStar inc. San Carlos, CA, USA). FlowSOM v1.18.0 analysis was done as described previously (*26*). Lineage- (negative for CD3/CD56/CD19) HLA-DR+ data were transformed using the *logicleTransform* function of the *flowCore* v1.52.1 R package, using default parameters (27). The SOM was trained for a 7x7 grid (49 clusters) with 2000 iterations for Lin-HLA-DR+ cells. Consensus hierarchical clustering was used to annotate clusters, based on the *ConsensusClusterPlus* v1.50.0 R package (*28*). Principal component analysis (PCA) analysis was done on normalized expression data from flowSOM using the *factoextra* v 1.0.7.999 R package.

RNA isolation and RNA sequencing

Total RNA from CD1c+ DC cell lysates from patients and controls was isolated using the AllPrep Universal Kit (Qiagen) on the QIAcube (Qiagen) according to the manufacturer's instructions. Library preparation and Illumina sequencing was performed on samples of the

discovery cohort at BGI (Hong Kong). RNA-seq libraries were generated with the TruSeq RNAseq RNA Library Prep Kit (Illumina Inc., Ipswich, MA, USA) and were sequenced using Illumina NextSeq 500 generating approximately 20 million 100bp paired end reads for each sample. For the replication cohort, RNA-seq libraries were generated by *GenomeScan* (Leiden, the Netherlands) with the TruSeq RNAseq RNA Library Prep Kit (Illumina Inc., Ipswich, MA, USA), and were sequenced using Illumina HiSeq 4000 generating ~20 million 150bp paired ended reads for each sample.

Power analysis

We conducted power analysis of the discovery cohort using the PROPER R package v 1.22.0 (*29*) with 100 simulations of the *build-in* RNA-seq count data from antigen presenting (B) cells from a cohort of 41 individuals (i.e., large biological variation as expected in our study) (*30*). Simulations parameters used the default of 20,000 genes and an estimated 10% of genes being differentially expressed. We detected 0.8 power to detect differentially expressed genes ($P<0.05$) at a $\log_2$(fold change)>1 for the smallest patient group (9 cases) and we considered the sample size reasonable for analysis.

Differential gene expression and statistical analysis

Quality check of the raw sequences was performed using the FastQC tool. Reads were aligned to the human genome (GRCh38 build 79) using STAR aligner (*31*) and the Python package HTSeq v0.6.1 was used to count the number of reads overlapping each annotated gene (32). We aligned the reads of the RNA sequencing data sets to 65,217 annotated *Ensemble Gene* IDs. Raw count data were fed into *DESeq2* v1.30.1(*33*) to identify differentially expressed genes (DEGs) between the four disease groups (AU, IU, BU, HC). Using DESeq2, we modelled the biological variability and overdispersion in expression data following a negative binomial distribution. We used Wald's test in each disease group versus control pair-wise comparison and *P* values were corrected by *DESeq2* package using the Benjamini-Hochberg Procedure. We constructed co-expression gene networks ($\beta = 6$) with the WGCNA v 1.70-3 R

package (34) using the cumulative uveitis-associated genes (P<0.05, n=6,794 genes) from all pairwise comparisons. We calculated the intersect between the modules constructed from the two cohorts and used Fisher's exact test to identify modules that exhibited significant overlap in genes. Gene expression data from *runx3*-knockout(KO) cDC2s, *notch2*-KO cDC2s, and inflammatory cDC2s were obtained from the NCBI Gene Expression Omnibus (accession numbers GSE48590 [2 wild-type [WT] CD11b+Esam+ splenic cDC2s versus 2 CD11b+Esam+ cDC2s from CD11c-DC-*Runx3*Δ mice], GSE119242 [2 untreated cDC2 versus untreated cDC2 from CD11c-Cre *notch2*f/f mice], GSE149619 [5 CD172+MAR1- cDC2s in mock condition vs 3 CD172+MAR1+ cDC2 in virus (flu) condition]) using GEO2R in the GEO database, which builds on the *GEOquery* v2.58.0 and *limma* R v 3.46 packages (*35,36).* RNA-seq data from the mouse bone marrow stromal cell line OP9 expressing NOTCH ligand DLL1 (OP9-DLL1)-driven cDC2 cultures (GSE110577, [2 sorted CD11c+MHCII+B220−CD11b+ cDC2 from bone marrow cultures with FLT3L for 7 days vs 2 sorted CD11c+MHCII+B220−CD11b+ cDC2 from bone marrow cultures with FLT3L + OP9-DLL1 cells for 7 days]) were analyzed using *DESeq2* and normalized count data plotted using the *plotCounts* function. RNA-seq count data from CD14+/- DC3 subsets (CD5-CD163+CD14-/CD5-CD163+CD14+ CD1c+ DCs) from patients with SLE and Systemic sclerosis were obtained via GEO (accession number: GSE136731) (*17*) and differential expression analysis was conducted using *DESeq2* v1.30.1. Gene set enrichment analysis was done using the *fgsea* R package v1.16.0 and data plotted using the *GSEA.barplot* function from the *PPInfer* v 1.16.0 R package (*37*). Gene sets for *runx3*-KO, *notch2*-KO, inflammatory cDC2s, and cDC2s from OP9-DLL1 bone marrow cultures were generated by taking the top or bottom percentiles of ranked [$-\log_{10}(P) \times \text{sign}(\log_2(\text{fold change}))$] genes from each data set as indicated.

Single cell-RNA seq analysis of aqueous humor.

Single cell RNA-seq (scRNA-seq) data from aqueous humor of 4 HLA-B27-positive anterior uveitis (identical to the AU group in this study) patients and control were obtained via Gene Expression Omnibus (GEO) repository with the accession code GSE178833. Data were

processed using the R package *Seurat* v4.1.0 (*38*) using R v4.0.3. We removed low-quality cells (<200 or >2500 genes and mitochondrial percentages <5%) and normalized the data using the *SCTransform()* function accounting for mitochondrial percentage and cell cycle score (*39*). Dimensionality reduction was achieved by adapting the original UMAP coordinates for each barcode as reported by *Kasper et al 2021* (see GSE178833). Samples from 4 (HLA-B27-positive) AU patients and the control were subjected to *scGate* v1.0.0 (*40*) using *CLEC10A* in our gating model to purify CD1c+ DCs in the scRNA seq dataset. We calculated module enrichment scores for the black module genes using the *UCell* R package v1.3.1 (*41*) (using genes with high module membership [-0.85< or >0.85, n=18) in cohort I, **Supplementary File 1G**) and clustered CD1c+DCs into positive and negative fractions.

Data and Code Availability

The data code (R markdown), bulk RNA-Seq datasets, flow cytometry dataset, and cytokine expression dataset described in this publication are available via https://dataverse.nl/ doi: https://doi.org/10.34894/9Q0FVO and deposited in NCBI's Gene Expression Omnibus accessible through GEO Series accession numbers GSE195501 and GSE194060.

Results

An CD1c+ DC transcriptome module is associated with non-infectious uveitis

We aimed to characterize the transcriptome of primary CD1c+ DCs from patients with non-infectious uveitis (**Figure 1A**). We isolated CD1c+ DC cells from blood of 28 adult patients with anatomically distinct types of non-infectious uveitis (**Table 1**) and 14 age- and sex-matched controls and studied the transcriptome of the highly purified CD1c+ DC cell fractions (median [interquartile range]% = 96[3]% pure, **Figure 1 - Figure Supplement 1**) by bulk RNA-sequencing (*RNA-seq*). We identified 678 unique differentially expressed genes (*Padj*<0.05) between uveitis subtypes and controls (**Supplementary File 1H**). Patient samples did not cluster according to clinical parameters of disease activity (e.g., cell grade in eye fluid, macular thickness) (**Figure 1 - Figure Supplement 2A-E**). In contrast, the expression profile of the

DEGs split the samples into clear patient and control groups in two-dimensional PCA subspace (**Figure 1B**). To detect a biologically relevant higher order organization of the transcriptome with sufficient resolution, we constructed co-expression networks by combining the DEGs with other uveitis-associated genes detected by differential expression analyses between the groups (P<0.05, n= 6,794 unique genes, **Supplementary File 1H**), which discerned 24 gene modules (**Figure 1C**). Inspection of the module's *eigengene* values across the samples revealed that the 'black' module (1,236 genes with 167 with *Padj*<0.05) was the largest and associated with uveitis, regardless of disease subtype (**Figure 1D, Figure 1 – Figure Supplement 2F**). Within the black module, transcripts encoding the chemokine receptors *CX3CR1* (Module Membership [MM] = 0.95, $P = 5.9 \times 10^{-22}$) and *CCR2* (MM = 0.92, $P = 1.8 \times 10^{-17}$) showed the highest module membership and thus best represent the expression pattern of the uveitis-associated module (**Supplementary File 1H**). Because these cell-surface receptors and other genes encoding cell-surface proteins in the black module (e.g., *ESAM*, *CLECL12A*) have been associated with distinct subsets of cDC2s (*42-45*), we focused on the 100 genes in the black module that encode cell-surface proteins (according to *surfaceome* predictor *SURFY*)(*46*) and their transcriptional regulation (**Supplementary File 1H**); In addition to *CX3CR1*, the scavenger receptor *CD36*, and Toll like receptor (TLR) family members *TLR1, TLR4, TLR6-8*, and *CD180*, all showed significantly (*Padj*<0.05) higher gene expression levels in CD1c+ DC cells of patients (**Figure 1E**). Eight transcription factors previously shown to be linked to distinct human CD1c+ DC subsets (*47*) were also detected in the black module, including *RUNX3, IRF8,* and *NFKB1* (**Figure 1E**).

The gene module encompassing *CX3CR1* and *CD36* has been linked to a population within the CD1c+ DC pool with a 'monocyte-like' transcriptome as well as inflammatory CD14+ monocytes, which cannot be distinguished by bulk RNA-seq analysis (*16,42,48*). Although we observed CD14-positive cells in our CD1c+ fractions, there was no difference between patient and control samples (**Figure 1F**), nor was *CD14* differentially expressed by RNA-seq (P > 0.05). Furthermore, *CD14* correlated weakly with the black module (Pearson correlation

coefficient = 0.25, **Figure 2 – Supplement 1A**). To test whether the black module was directly dependent on CD14 surface expression by CD1c+ DCs, we FACS-isolated blood CD14+ and CD14- fractions from CD1c+ DCs of six healthy donors (**Figure 2A**). RT-qPCR analysis revealed that the expression of a panel of key genes of the black module, including *CD36*, *CCR2*, *CX3CR1*, and *RUNX3* were not significantly different between CD14+ CD1c+ DCs and CD14- CD1c+ DCs (**Figure 2B**), with the exception of *TLR7* (**Figure 2 - Figure Supplement 1B**). In addition, RNA-sequencing data of FACS-sorted CD14+ CD1c+ DCs and CD14- CD1c+ DCs fractions purified from PBMCs of patients with *type IFN-I diseases* SLE and *Systemic Sclerosis* further verified that - unlike *CD14* - the majority of genes of the black module (including *CD36*, *CX3CR1*, *CCR2*, and *RUNX3*) were not significantly affected by CD14 surface expression during chronic inflammation (**Figure 2C**). We concluded that the black module was not fully dependent on CD14 expression, which would allow us to test if the association between the black module and non-infectious uveitis could also be perceived in the CD14- CD1c+ DC fraction. To ascertain that we could attribute the black module to CD1c+ DCs by bulk RNA-seq analyses, we next purified CD14-*negative* CD1c+ DCs by FACS from an independent cohort of 36 patients and controls and performed bulk RNA-seq (**Figure 2D** and **Supplementary File 1I**). Co-expression network analysis of the uveitis-associated genes (n=2,016 genes at $P<0.05$) from the second cohort distinguished six gene modules. Three modules exhibited a significant number of overlapping co-expressed genes with the black module from the discovery cohort (**Figure 2E**). The gene expression levels for these replicated co-expressed genes were nearly identical between the two cohorts (*Spearman R*=0.95, **Figure 2 - Figure Supplement 1C**), but with a clearly lower sensitivity to replicate relatively lower expressed genes (i.e., likely due to ~3-fold lower cell yield after the removal of CD14+ cells by FACS-sorting compared to cohort I, see *Methods*). Regardless, in total, 147 differentially co-expressed genes of the black module in the first cohort were also co-expressed in the second cohort (**Figure 2F**), of which 94% of these co-expressed genes also showed consistent direction of effect (e.g., upregulated in both cohorts)(**Figure 2F**, **Supplementary File 1J)**, which substantiates this gene module as a robust and *bona fide* transcriptional feature of

CD1c+ DCs in human non-infectious uveitis. Among the 147 genes, we replicated *CX3CR1*, *CD36*, *CCR2*, *CCR5*, *TLR-6,-7,-8*, *CD180* (**Figure 2H**), but also *TNFRSF1A* (the main TNF-alpha receptor), *CYBB,* (critically involved in T cell activation by DCs in autoimmune models) (*49*), and transcription factors *RUNX3*, *IRF8*, and *NFKBI* associated with cDC2 subsets (*18,47*). Note, *CCR2* and *CX3CR1* also showed high module membership in the second cohort (**Supplementary File 1J**), and were also significantly associated with non-infectious uveitis after correction for multiple testing (*Padj*<0.05, **Supplementary File 1J**). Collectively, these data show a skewed transcriptional signature in blood CD1c+ DCs of non-infectious uveitis patients.

NOTCH2-RUNX3 signaling controls the CD1c+ DC gene module of non-infectious uveitis

Among the 147 genes with consistent direction of effect in both cohorts, we noticed *RUNX3*, *IRF8*, and *NFKB1* as potential transcriptional regulators for the black module (**Figure 2H**). Note that *RUNX3, IRF8,* and *NFKB1* also clustered into a single transcriptomic cluster in single cell analysis of human CD1c+ DC subsets by Brown and associates (*47*). Because loss of RUNX3 in mononuclear phagocytes (i.e., cDC2s) has been linked with chronic inflammation (*50*), we hypothesized that the signaling that involves the transcription factor *RUNX3* may promote the transcriptomic signature that characterize CD1c+ DCs of patients.

Efforts to study the effects of siRNA-mediated knockdown or CRISPR-Cas9-mediated knockout (KO) of *RUNX3* in CD1c+ DCs were unsuccessful (no knock-down or knock-out of *RUNX3* achieved). Therefore, we analyzed gene expression data of the cDC2s (murine equivalent of human CD1c+ DCs) cells from CD11c-DC-*Runx3*Δ mice (*51*). Loss of *runx3* in murine cDC2s resulted in a gene expression profile that considerably recapitulates the black module (**Figure 3A**). In detail, we detected enrichment for many genes that are upregulated in *runx3*-KO cDCs2, including *cd36*, *ccr2*, and *cx3cr1* by gene-set enrichment analysis (GSEA) (**Figure 3B**). This supports our hypothesis that the 'monocyte-like' signature genes (i.e. *CD36*, *CX3CR1*, *CCR2*) are regulated by RUNX3. Indeed, RUNX3 directly binds the promoter of *CD36* and negatively regulates its expression in myeloid cells (*52*). Importantly, overnight

stimulation of MACS-sorted CD1c+ DCs by various key myeloid cytokines or Toll-like receptor (TLR) ligands did not result in a decrease in expression of *RUNX3* nor in a concordant increase in *CD36* expression, suggesting that the observed gene signature in the CD1c+ DC pool is unlikely to reflect an activation continuum (**Figure 3C**). In fact, TLR-stimulation (with LPS, LTA, or R848) resulted in a strong upregulation of *RUNX3* and downregulation of CD36, which is the opposite of the expression pattern detected in patients. Also, overnight stimulation with cytokines GM-CSF and IFN-alpha that are implicated in the promotion of specific cDC2 subsets (*19,20*) did not decrease the expression of *RUNX3* (**Figure 3C**). In general, the transcriptional signature of non-infectious uveitis did not resemble the gene signature of *in vivo* activated cDC2s (termed 'inflammatory' cDC2s' [*infcDC2s*]) (*53*). However, we did observe a significant positive enrichment score for genes down-regulated in infcDC2s in the transcriptome of IU patients (**Figure 3A** and **3B**).

Because murine studies underscored a *notch*-dependent divergence of cDC2 subsets (*42,54*), we reasoned that the CD1c+ DC transcriptional signature driven by *RUNX3* would rely on NOTCH2 signaling. To explore this, we investigated the transcriptome of dendritic cells of notch2Δ-CD11c mice (*55*). In agreement with the expression data of the CD11c-DC-Runx3Δ mice, loss of Notch2 resulted in up regulation of *ccr2*, *cd36*, *cx3cr1*, and decreased expression of *runx3* (**Figure 3A**), and we detected enrichment for genes upregulated in *notch2*-KO cDCs2 (**Figure 3B**). This supports that NOTCH2 is upstream of RUNX3 and mediates the transcriptomic characteristics of blood CD1c+ DCs of non-infectious uveitis. These findings were further strengthened in reanalysis of transcriptomic data of murine bone marrow progenitors cultured for 7 days with OP9 stromal cells that express the NOTCH2 ligand DLL1 or OP-9 cells without DLL1 (*56,57*). This analysis revealed that *notch2*-controlled genes were enriched in the transcriptome of CD1c+ DCs of patients and that notch2-signalling governs the expression of *cd36, ccr2, and cx3cr1* in cDC2s (**Figure 3D** and **Figure 3E).** Collectively, these observations support that *NOTCH2-RUNX3* signaling promotes the black module gene profile of CD1c+ DCs in human non-infectious uveitis.

CD36+CX3CR1+ DC3 are diminished in peripheral blood of non-infectious uveitis patients

We reasoned that the transcriptomic signature of the CD1c+ DC pool in patients may be an impression of changes in the proportions of CD1c+ DC subsets in blood. To allow unbiased identification of CD1c+ DC phenotypes, we first used flow cytometry analysis to identify CD1c+ DC clusters in peripheral blood mononuclear cells (PBMCs) samples from 26 cases and 11 controls. We designed a panel based on the black module (CD36, CX3CR1, CCR2, and CD180), surface markers previously linked to CD1c+ DC subsets, but that were *not* in the black module (CD5, and CD163) (*17, 58*), and classical CD1c+ DC markers (CD1c and CD11c). FlowSOM (*59*) was used on HLA-DR+ and lineage (CD3/CD19/CD56)- PBMCs to cluster cells into a predetermined number of 49 clusters (7x7 grid) to facilitate unbiased detection of CD1c+ DC phenotypes in blood. The analysis with flowSOM clearly distinguished four (Lin-HLA-DR+CD11c+)CD1c+ DC clusters (cluster number 22, 37, 44, and 45)(**Figure 4A** and **Figure 4 – Supplement 1A and B**). We extracted the data for these four CD1c+ DC clusters and conducted *principal component analysis* (PCA). The PCA biplot identified CD5 and CD163 as top loadings, which defines the *DC2* (cluster 45) and *DC3* subsets (cluster 22, 37, and 44) (*17*) (**Figure 4B**). Among the identified clusters, we detected a significant reduction in the frequency of cluster 44 in patients compared to controls (*Welch T-test*, P = 0.03, **Figure 4C and D**). Although cluster 22 and cluster 44 are both (CD5-CD163+)CD14+ DC3s (**Figure 4 – Supplement 1C**), cluster 44 distinguished itself by relatively higher CD36 and CX3CR1, which is in agreement with our RNA-seq analysis (**Figure 4E** and **4F**). We validated by manual gating that cluster 44 represents the CD36+CX3CR1+ fraction of CD1c+ DCs in peripheral blood (**Figure 4G**). Comparison between patients and controls corroborated that the frequency of manual gated CD36+CX3CR1+ DC3s were decreased in the blood of non-infectious uveitis patients (Welch *t*-test, P = 0.03, **Figure 4H** and **4I**). We established that CD36+CX3CR1+ DC3s are a subpopulation of CD14+DC3s (**Figure 4J) (Figure 4 – Supplement 2**), indicating a previously unrecognized phenotypic diversity among inflammatory CD14+ DC3s (*17*).

Together, these results demonstrate that CD36+CX3CR1+ DC3s were diminished in the blood of patients with non-infectious uveitis.

CD36+CX3CR1+DC3s secrete high levels of pro-inflammatory cytokines

Next, we were interested if the CD36+CX3CR1+CD1c+ DC subset was functionally different from other CD1c+ DC subsets. To this end, we freshly sorted primary human CD1c+ DC subsets based on the surface expression of CD36 and CX3CR1, of which double-positive and double-negative subsets could be sorted from the selected healthy subjects in sufficient numbers for analysis (**Figure 5 – Figure Supplement 1**). Since CD36 is required for lipoteichoic acid (LTA) induced cytokine production (*60*), we overnight stimulated the CD1c+ subsets with LTA. Interleukin (IL)-23, a cytokine potently produced by CD1c+ DCs in general, was equally strong secreted by both subsets of CD1c+ DCs (**Figure 5A**). To assess the secretome of the CD1c+ DC subsets in more detail, we profiled the supernatants of LTA-stimulated CD1c+ DC subsets for additional soluble immune mediators (**Supplementary File 1E**): The CD1c+ DC subsets could be distinguished based on the secreted protein profile (**Figure 5B**), of which the levels of TNF-alpha, IL-6, VEGF-A, and TNFR1 showed significant differences between the subsets (**Figure 5C**). These results show that CD1c+ DC subsets defined on the basis of surface co-expression of CD36 and CX3CR1 show a differential capacity to secrete pro-inflammatory mediators that participate in the pathophysiology of human non-infectious uveitis.

CD36+ CX3CR1+ DC3s infiltrate the eye during non-infectious.

We speculated that the decrease in blood CD36+CX3CR1+ CD1c+ DCs was in part the result of migration of these cells to peripheral tissues (lymph nodes) and that these cells may infiltrate the eye during active uveitis. We used single-cell RNA sequencing data of eye fluid biopsies of patients (*61*) and identified CD1c+ DCs by cells using the CD1c+ DC specific tissue-marker *CLEC10A* (*20*,*62*)(**Figure 6A**). Next, we determined the relative expression of the black module in these cells by calculating the module enrichment for each cell (i.e., *UCell score* for

genes with high module membership, **Supplementary File 1G**) and cluster CD1c+ DCs into black-module-*negative* and black-module-*positive* subpopulations(**Figure 6B).** In line with our bulk RNA-seq data, eye-infiltrating black-module-*positive* CD1c+ DCs expressed relatively higher levels of *CD36, CX3CR1, CCR2,* and lower levels of *RUNX3* (but comparable levels of *CD14*) compared to black module-negative CD1c+DCs and therefore represent CD36+CX3CR1+DC3s (**Figure 6C**). CD36+CX3CR1+DC3s were found in relatively higher abundance in eyes of non-infectious uveitis patients (**Figure 6D**). In summary, we conclude that CD36+ CX3CR1+ DC3s infiltrate the eye during active non-infectious uveitis.

Discussion

In this study of non-infectious uveitis patients and controls, we identified and replicated a robust and *bona fide* transcriptional module in CD1c+ DCs. We were able to track back the network to a cytokine-producing CD36+CX3CR1+ CD1c+ DC subset that was diminished in peripheral blood but infiltrate the eyes of patients with non-infectious uveitis.

Using data from genetic models, we show that reciprocal expression of the gene network associated with non-infectious uveitis relies on transcription factors NOTCH2 and RUNX3. In detail, we showed that NOTCH2 signaling regulates the expression of *CD36*, and *CX3CR1* via *RUNX3* in CD1c+ DCs and that this recapitulates the (black module) gene signature of non-infectious uveitis.

Brown *et al*., (*47*) recently showed that in human blood CD1c+ DCs, differential expression of transcription factors, including *RUNX3*, *IRF8*, and *NFKB1* (which were all in the transcriptional signature of CD1c+ DCs of patients) delineate CD1c+ DC subsets. Our observation that these transcription factors were differentially co-expressed support that the gene expression changes identified in uveitis patients were mediated by compositional changes in discrete subsets with reciprocal gene expression patterns (*16*).

Other preceding studies into human CD1c+ DCs revealed functionally distinct subsets termed “DC2” and “DC3”, with the DC3 showing both transcriptomic features reminiscent of cDC2s and monocytes - such as elevated *CD36* and *CD14* levels (*16,17*). DC3s also have distinct

developmental pathways and transcriptional regulators compared to DC2 (*16-18,20*). Recently, Cytlak and associates revealed that lower expression of *IRF8* is linked to DC3 (*18*), a transcription factor that was also decreased in non-infectious uveitis. Dutertre and co-workers (*17*) showed that the phenotype of peripheral blood CD1c+ DCs can be further segregated according to the expression of CD163 and CD5, with "DC3" cells being characterized as CD5-CD163- or CD5-CD163+cells and "DC2" as CD5+CD163 cells. We show that (CD5-CD163+) DC3 can also be further segregated based on surface expression of CD36 and CX3CR1. Importantly, we show that (CD5−CD163+) CD14+ DC3s (previously termed "inflammatory" CD14+ DC3 cells [*17*]), comprise of two subpopulations defined by CD36 and CX3CR1, of which the (CD14+) CD36+CX3CR1+DC3 are altered in frequency in blood in non-infectious uveitis, but the CD14+CD36+CX3CR1- DC3s are not (**Figure 4J**). Single-cell analysis supported this diversity in CD14+ DC3s by showing that eye-infiltrating CD1c+ DCs that were enriched for the uveitis-associated (black) gene module exhibited relatively higher levels of *CD36, CX3CR1, CCR2,* and lower levels of *RUNX3*, but not *CD14*. Although we demonstrate that CD36+CX3CR1+ cells also express CD14, as a proof of concept, we demonstrated that the association of the black module with non-infectious uveitis can even be perceived in CD14- CD1c+ DCs, emphasizing that this gene circuit represent a previously unrecognized DC3 cell state and heterogeneity in inflammatory CD14+DC3s. Since CD36+ CX3CR1+ DC3s define phenotypically discrete populations of CD14+ DC3 in peripheral blood and inflamed tissue, it would be interesting to determine the functional program of these cells in other inflammatory conditions and cancer. When considering the DC3 population as a whole for comparison to previous studies, patients with *Systemic lupus erythematosus* (SLE) display accumulation of CD5-CD163+ DC3s in blood (*17*), while this population of DC3 cells (CD5-CD163+CD1c+ DCs) was decreased in non-infectious uveitis patients. The differences between non-infectious uveitis and SLE may be related to distinct (i.e., opposite) immunopathological mechanisms; Type I interferons drive the maturation of cDC2s into "inflammatory cDC2s" (infcDC2s)(*53*) and can induce CD1c+ DCs to express a distinct set of surface-receptors (*19*). The type I interferon (IFN)-α drives immunopathology of

SLE and administration of type I interferon therapy can induce *lupus-like* disease (*22,23*). In favor of attributing the seemingly contrasting observations in blood CD1c+ subsets between SLE and non-infectious uveitis to distinct biology is the fact that, in contrast to elevated IFN-α in patients with SLE, in non-infectious uveitis patient's disease exacerbations correlate with reduced blood type I IFN concentrations (*21,63*). In addition, we demonstrated that the transcriptional signature of CD1c+ DCs in non-infectious uveitis was not positively enriched for transcriptomic features of IFN-driven cDC2 subset (**Figure 3**).

This also indicates that unlike SLE (*64*), changes of the CD1c+ DC peripheral blood pool in non-infectious uveitis are not driven by increased type I interferon signaling (*21*), but rather by yet unspecified pathological molecular pathways. This is supported by the fact that in our stimulation experiments, IFN alpha did not induce the uveitis-associated gene signature in CD1c+ DCs (**Figure 3**) and that type I interferon therapy inhibits non-infectious uveitis (*21*). However, an argument against this is that we detected enrichment for genes down-regulated in infcDC2s (*53*) in IU patients. In detail, although not all statistically significant, genes such as *ccr2*, *cd36*, *cx3r1* showed a relative decrease in expression, while *runx3* showed a relative increase in expression in the transcriptome of *infcDC2s* versus "non-inflammatory" cDC2s (based on GSE149619). In other words, this suggest that the profile of *infcDC2s* within the CD1c+DC pool was 'decreased' in IU patients, which is in line with the decrease in the frequency of CD5-CD163 DC3s as a whole or the inflammatory cytokine-secreting CD36+CX3CR1+ DC3 subset in patients with non-infectious uveitis. One possible explanation for the decrease in this subset may be that in the systemic condition SLE 'inflammatory' DC3s 'accumulate' in blood, while in non-infectious uveitis this population exits the circulation to infiltrate secondary lymphoid tissues and ocular structures to mediate eye inflammation. Indeed, we show by single cell analysis of ocular fluids of patients the infiltration of CD36+ CX3CR1+ DC3s in the eye during non-infectious uveitis (**Figure 6**). We further showed that CD36+CX3CR1+ DC3s secreted more inflammatory cytokines, such as tumor necrosis factor alpha (TNF-α) and IL-6. This is significant, because anti-TNF and anti-IL-6 therapy are both

(highly) effective for treatment of non-infectious uveitis (*65*), which underlines the significance of the TNF-producing DC3 subset identified in this study for the pathophysiology of non-infectious uveitis. Ideally longitudinal data are used to follow the dynamics of this population in patients in relation to disease activity, which is a limitation of the current study.

Other disease modifying factors possibly affect the CD1c+ DC pool in uveitis patients. In mice, antibiotic treatment to experimentally disturb the microbiota affects a cDC2 subset phenotypically similar to CD1c+ DCs and decreases their frequency in the intestine of mice, which suggests microbiota-dependent signals involved in the maintenance of cDC2 subsets (*47*). This is especially interesting in light of growing evidence that microbiota dependent signals cause autoreactive T cells to trigger uveitis (*66*), which makes it tempting to speculate that gut-resident cDC2 subsets contribute to the activation of T cells in uveitis models. Dietary components can influence subsets of intestinal dendritic cells (*67*). Regardless, most likely, an ensemble of disease modulating factors is involved. For example, myeloid cytokines, such as GM-CSF, contribute to autoimmunity of the eye (*68*) and GM-CSF has been shown to stimulate the differentiation of human CD1c+ subset from progenitors (*20*). However, GM-CSF signaling in conventional dendritic cells has a minor role in the inception of EAU (*69*). Our data supports that stimulation of CD1c+ subsets with GM-CSF or TLR ligands does not induce the transcriptional features of CD1c+ DCs during non-infectious uveitis, which is in line with previous observations that support that stimulated cDC2s do not convert from one into another subset (*20*). Note that key transcription factors (e.g. *RUNX3*) defining the here identified CD1c+ subsets are definitely affected by TLR stimulation, but the overall transcriptomic program of activated CD1c+ DCs is distinct (**Figure 3**).

Better understanding of the changes in the CD1c+ DC pool during human non-infectious uveitis will help develop strategies to pharmacologically influence putative disease pathways involved at an early disease stage, which may lay the foundation for the design of effective strategies to halt progress towards severe visual complications or blindness. Perhaps targeting CD1c+

DCs may be achieved by dietary (microbiome) strategies and provide relatively safe preventive strategies for noninfectious uveitis.

In conclusion, we discovered a CD36+CX3CR1+CD1c+ DC subset that decreased in the peripheral blood of patients with non-infectious uveitis. The fact that this population secretes high levels of TNF-alpha, is decreased in the circulation of patients, while CD1c+ DCs expressing *CD36* and *CX3CR1* accumulate locally in uveitis patients may not only explains the therapeutic benefit of TNF inhibition for non-infectious uveitis, it also opens new avenues for therapeutic targeting to prevent blindness due to non-infectious uveitis.

Supplementary Materials

Figure Supplements

Supplementary File 1

References

1. Thorne JE, Suhler E, Skup M, Tari S, Macaulay D, Chao J, Ganguli A. Prevalence of Noninfectious Uveitis in the United States: A Claims-Based Analysis. JAMA Ophthalmol. 2016 Nov 1;134(11):1237-1245.
2. Suttorp-Schulten MS, Rothova A. The possible impact of uveitis in blindness: a literature survey. Br J Ophthalmol. 1996 Sep;80(9):844-8.
3. Lee RW, Nicholson LB, Sen HN, Chan CC, Wei L, Nussenblatt RB, Dick AD. Autoimmune and autoinflammatory mechanisms in uveitis. Semin Immunopathol. 2014 Sep;36(5):581-94.
4. Caspi RR. A look at autoimmunity and inflammation in the eye. J Clin Invest. 2010 Sep;120(9):3073-83.
5. Kuiper JJW, Venema WJ. HLA-A29 and Birdshot Uveitis: Further Down the Rabbit Hole. Front Immunol. 2020 Nov 11;11:599558.
6. Huang XF, Li Z, De Guzman E, et al. Genomewide Association Study of Acute Anterior Uveitis Identifies New Susceptibility Loci. Invest Ophthalmol Vis Sci. 2020;61(6):3. doi:10.1167/iovs.61.6.3
7. Kuiper JJW, Setten JV, Devall M, Cretu-Stancu M, Hiddingh S, Ophoff RA, Missotten TOAR, Velthoven MV, Den Hollander AI, Hoyng CB, James E, Reeves E, Cordero-Coma M, Fonollosa A, Adán A, Martín J, Koeleman BPC, Boer JH, Pulit SL, Márquez A, Radstake TRDJ. Functionally distinct ERAP1 and ERAP2 are a hallmark of HLA-A29-(Birdshot) Uveitis. Hum Mol Genet. 2018 Dec 15;27(24):4333-4343. doi: 10.1093/hmg/ddy319. PMID: 30215709; PMCID: PMC6276832.
8. Márquez A, Cordero-Coma M, Martín-Villa JM, Gorroño-Echebarría MB, Blanco R, Díaz Valle D, Del Rio MJ, Blanco A, Olea JL, Cordero Y, Capella MJ, Díaz-Llopis M, Ortego-Centeno N, Ruiz-Arruza I, Llorenç V, Adán A, Fonollosa A, Ten Berge J, Atan D, Dick AD, De Boer JH, Kuiper J, Rothova A, Martín J. New insights into the genetic component of non-infectious uveitis through an Immunochip strategy. J Med Genet. 2017 Jan;54(1):38-46. doi: 10.1136/jmedgenet-2016-104144. Epub 2016 Sep 8. PMID: 27609017.
9. Chen M, Liang D, Zuo A, Shao H, Kaplan HJ, Sun D. An A2B Adenosine Receptor Agonist Promotes Th17 Autoimmune Responses in Experimental Autoimmune Uveitis (EAU) via Dendritic Cell Activation. PLoS One. 2015 Jul 6;10(7):e0132348.
10. Fu Q, Man X, Wang X, Song N, Li Y, Xue J, Sun Y, Lin W. CD83+ CCR7+ NK cells induced by interleukin 18 by dendritic cells promote experimental autoimmune uveitis. J Cell Mol Med. 2019 Mar;23(3):1827-1839.
11. Wang B, Tian Q, Guo D, Lin W, Xie X, Bi H. Activated γδ T Cells Promote Dendritic Cell Maturation and Exacerbate the Development of Experimental Autoimmune Uveitis (EAU) in Mice. Immunol Invest. 2021 Feb;50(2-3):164-183.
12. Chen P, Urzua CA, Knickelbein JE, Kim JS, Li Z, Hannes S, Kuo D, Chaigne-Delalande B, Armbrust K, Tucker W, Liu B, Agrón E, Sen HN, Nussenblatt RB. Elevated CD1c+ Myeloid Dendritic Cell Proportions

Associate With Clinical Activity and Predict Disease Reactivation in Noninfectious Uveitis. Invest Ophthalmol Vis Sci. 2016 Apr;57(4):1765-72. doi: 10.1167/iovs.15-18357. PMID: 27070110; PMCID: PMC4849533.
13. Chen P, Denniston A, Hannes S, Tucker W, Wei L, Liu B, Xiao T, Hirani S, Li Z, Jawad S, Si H, Lee RW, Sen HN, Nussenblatt RB. Increased CD1c+ mDC1 with mature phenotype regulated by TNFα-p38 MAPK in autoimmune ocular inflammatory disease. Clin Immunol. 2015 May;158(1):35-46. doi: 10.1016/j.clim.2015.03.002. Epub 2015 Mar 14. PMID: 25784146; PMCID: PMC4420697.
14. Chen P, Tucker W, Hannes S, Liu B, Si H, Gupta A, Lee RW, Sen HN, Nussenblatt RB. Levels of blood CD1c+ mDC1 and CD1chi mDC1 subpopulation reflect disease activity in noninfectious uveitis. Invest Ophthalmol Vis Sci. 2014 Dec 16;56(1):346-52.
15. O'Rourke M, Fearon U, Sweeney CM, Basdeo SA, Fletcher JM, Murphy CC, Canavan M. The pathogenic role of dendritic cells in non-infectious anterior uveitis. Exp Eye Res. 2018 Aug;173:121-128.
16. Villani AC, Satija R, Reynolds G, et al. Single-cell RNA-seq reveals new types of human blood dendritic cells, monocytes, and progenitors. Science. 2017;356(6335):eaah4573. doi:10.1126/science.aah4573
17. Dutertre CA, Becht E, Irac SE, Khalilnezhad A, Narang V, Khalilnezhad S, Ng PY, van den Hoogen LL, Leong JY, Lee B, Chevrier M, Zhang XM, Yong PJA, Koh G, Lum J, Howland SW, Mok E, Chen J, Larbi A, Tan HKK, Lim TKH, Karagianni P, Tzioufas AG, Malleret B, Brody J, Albani S, van Roon J, Radstake T, Newell EW, Ginhoux F. Single-Cell Analysis of Human Mononuclear Phagocytes Reveals Subset-Defining Markers and Identifies Circulating Inflammatory Dendritic Cells. Immunity. 2019 Sep 17;51(3):573-589.e8. doi: 10.1016/j.immuni.2019.08.008. Epub 2019 Aug 29. PMID: 31474513.
18. Cytlak U, Resteu A, Pagan S, et al. Differential IRF8 Transcription Factor Requirement Defines Two Pathways of Dendritic Cell Development in Humans. Immunity. 2020;53(2):353-370.e8. doi:10.1016/j.immuni.2020.07.003
19. Girard M, Law JC, Edilova MI, Watts TH. Type I interferons drive the maturation of human DC3s with a distinct costimulatory profile characterized by high GITRL. Sci Immunol. 2020 Nov 13;5(53):eabe0347.
20. Bourdely P, Anselmi G, Vaivode K, Ramos RN, Missolo-Koussou Y, Hidalgo S, Tosselo J, Nuñez N, Richer W, Vincent-Salomon A, Saxena A, Wood K, Lladser A, Piaggio E, Helft J, Guermonprez P. Transcriptional and Functional Analysis of CD1c+ Human Dendritic Cells Identifies a CD163+ Subset Priming CD8+CD103+ T Cells. Immunity. 2020 Aug 18;53(2):335-352.e8.
21. Wang W, Chong WP, Li C, Chen Z, Wu S, Zhou H, Wan Y, Chen W, Gery I, Liu Y, Caspi RR, Chen J. Type I Interferon Therapy Limits CNS Autoimmunity by Inhibiting CXCR3-Mediated Trafficking of Pathogenic Effector T Cells. Cell Rep. 2019 Jul 9;28(2):486-497.e4
22. Rönnblom LE, Alm GV, Oberg KE. Autoimmunity after alpha-interferon therapy for malignant carcinoid tumors. Ann Intern Med. 1991 Aug 1;115(3):178-83.
23. Rönnblom LE, Alm GV, Oberg KE. Possible induction of systemic lupus erythematosus by interferon-alpha treatment in a patient with a malignant carcinoid tumour. J Intern Med. 1990 Mar;227(3):207-10.
24. Jabs DA, Nussenblatt RB, Rosenbaum JT; Standardization of Uveitis Nomenclature (SUN) Working Group. Standardization of uveitis nomenclature for reporting clinical data. Results of the First International Workshop. Am J Ophthalmol. 2005 Sep;140(3):509-16.
25. Bakker DS, de Graaf M, Nierkens S, Delemarre EM, Knol E, van Wijk F, de Bruin-Weller MS, Drylewicz J, Thijs JL. Unraveling heterogeneity in pediatric atopic dermatitis: Identification of serum biomarker based patient clusters. J Allergy Clin Immunol. 2022 Jan;149(1):125-134. doi: 10.1016/j.jaci.2021.06.029. Epub 2021 Jul 6. PMID: 34237306.
26. Laban KG, Rijken R, Hiddingh S, Mertens JS, van der Veen RLP, Eenhorst CAE, Pandit A, Radstake TRDJ, de Boer JH, Kalmann R, Kuiper JJW. cDC2 and plasmacytoid dendritic cells diminish from tissues of patients with non-Hodgkin orbital lymphoma and idiopath
27. Ellis B, Haaland P, Hahne F, Le Meur N, Gopalakrishnan N, Spidlen J, Jiang M, Finak G (2020). flowCore: flowCore: Basic structures for flow cytometry data. R package version 2.2.0.
28. Wilkerson, D. M, Hayes, Neil D (2010). “ConsensusClusterPlus: a class discovery tool with confidence assessments and item tracking.” Bioinformatics, 26(12), 1572-1573.
29. Wu H, Wang C, Wu Z. PROPER: comprehensive power evaluation for differential expression using RNA-seq. Bioinformatics. 2015 Jan 15;31(2):233-41.
30. Cheung VG, Nayak RR, Wang IX, Elwyn S, Cousins SM, Morley M, Spielman RS. Polymorphic cis- and trans-regulation of human gene expression. PLoS Biol. 2010 Sep 14;8(9):e1000480.
31. Dobin A, Davis CA, Schlesinger F, Drenkow J, Zaleski C, Jha S, Batut P, Chaisson M, Gingeras TR. STAR: ultrafast universal RNA-seq aligner. Bioinformatics. 2013 Jan 1;29(1):15-21.
32. Anders S, Pyl PT, Huber W. HTSeq--a Python framework to work with high-throughput sequencing data. Bioinformatics. 2015 Jan 15;31(2):166-9.
33. Love MI, Huber W, Anders S. Moderated estimation of fold change and dispersion for RNA-seq data with DESeq2. Genome Biol. 2014;15(12):550.
34. Langfelder P, Horvath S. WGCNA: an R package for weighted correlation network analysis. BMC Bioinformatics. 2008 Dec 29;9:559.
35. Davis S, Meltzer PS. GEOquery: a bridge between the Gene Expression Omnibus (GEO) and BioConductor. Bioinformatics. 2007 Jul 15;23(14):1846-7.
36. Ritchie ME, Phipson B, Wu D, Hu Y, Law CW, Shi W, Smyth GK. limma powers differential expression analyses for RNA-sequencing and microarray studies. Nucleic Acids Res. 2015 Apr 20;43(7):e47.

37. Jung D, Ge X (2020). PPInfer: Inferring functionally related proteins using protein interaction networks. R package version 1.16.0.
38. Stuart T, Butler A, Hoffman P, Hafemeister C, Papalexi E, Mauck WM 3rd, Hao Y, Stoeckius M, Smibert P, Satija R. Comprehensive Integration of Single-Cell Data. Cell. 2019 Jun 13;177(7):1888-1902.e21. doi: 10.1016/j.cell.2019.05.031. Epub 2019 Jun 6. PMID: 31178118; PMCID: PMC6687398.
39. Hafemeister C, Satija R. Normalization and variance stabilization of single-cell RNA-seq data using regularized negative binomial regression. Genome Biol. 2019 Dec 23;20(1):296. doi: 10.1186/s13059-019-1874-1. PMID: 31870423; PMCID: PMC6927181.
40. Andreatta M, Berenstein AJ, Carmona SJ. scGate: marker-based purification of cell types from heterogeneous single-cell RNA-seq datasets. Bioinformatics. 2022 Mar 8;38(9):2642–4. doi: 10.1093/bioinformatics/btac141. Epub ahead of print. PMID: 35258562; PMCID: PMC9048671.
41. Andreatta M, Carmona SJ. UCell: Robust and scalable single-cell gene signature scoring. Comput Struct Biotechnol J. 2021 Jun 30;19:3796-3798. doi: 10.1016/j.csbj.2021.06.043. PMID: 34285779; PMCID: PMC8271111.
42. Lewis KL, Caton ML, Bogunovic M, Greter M, Grajkowska LT, Ng D, Klinakis A, Charo IF, Jung S, Gommerman JL, Ivanov II, Liu K, Merad M, Reizis B. Notch2 receptor signaling controls functional differentiation of dendritic cells in the spleen and intestine. Immunity. 2011 Nov 23;35(5):780-91. doi: 10.1016/j.immuni.2011.08.013. Epub 2011 Oct 20. PMID: 22018469; PMCID: PMC3225703.
43. Kasahara S, Clark EA. Dendritic cell-associated lectin 2 (DCAL2) defines a distinct CD8α- dendritic cell subset. J Leukoc Biol. 2012 Mar;91(3):437-48. doi: 10.1189/jlb.0711384. Epub 2011 Dec 6. PMID: 22147811; PMCID: PMC3289397.
44. Fujita K, Chakarov S, Kobayashi T, Sakamoto K, Voisin B, Duan K, Nakagawa T, Horiuchi K, Amagai M, Ginhoux F, Nagao K. Cell-autonomous FLT3L shedding via ADAM10 mediates conventional dendritic cell development in mouse spleen. Proc Natl Acad Sci U S A. 2019 Jul 16;116(29):14714-14723. doi: 10.1073/pnas.1818907116. Epub 2019 Jul 1. PMID: 31262819; PMCID: PMC6642353.
45. Nakano H, Lyons-Cohen MR, Whitehead GS, Nakano K, Cook DN. Distinct functions of CXCR4, CCR2, and CX3CR1 direct dendritic cell precursors from the bone marrow to the lung. J Leukoc Biol. 2017 May;101(5):1143-1153.
46. Bausch-Fluck D, Goldmann U, Müller S, van Oostrum M, Müller M, Schubert OT, Wollscheid B. The in silico human surfaceome. Proc Natl Acad Sci U S A. 2018 Nov 13;115(46):E10988-E10997.
47. Brown CC, Gudjonson H, Pritykin Y, Deep D, Lavallée VP, Mendoza A, Fromme R, Mazutis L, Ariyan C, Leslie C, Pe'er D, Rudensky AY. Transcriptional Basis of Mouse and Human Dendritic Cell Heterogeneity. Cell. 2019 Oct 31;179(4):846-863.e24.
48. Schrøder M, Melum GR, Landsverk OJ, Bujko A, Yaqub S, Gran E, Aamodt H, Bækkevold ES, Jahnsen FL, Richter L. CD1c-Expression by Monocytes - Implications for the Use of Commercial CD1c+ Dendritic Cell Isolation Kits. PLoS One. 2016 Jun 16;11(6):e0157387.
49. Keller CW, Kotur MB, Mundt S, Dokalis N, Ligeon LA, Shah AM, Prinz M, Becher B, Münz C, Lünemann JD. CYBB/NOX2 in conventional DCs controls T cell encephalitogenicity during neuroinflammation. Autophagy. 2021 May;17(5):1244-1258. doi: 10.1080/15548627.2020.1756678. Epub 2020 May 13. PMID: 32401602; PMCID: PMC8143233.
50. Hantisteanu S, Dicken Y, Negreanu V, Goldenberg D, Brenner O, Leshkowitz D, Lotem J, Levanon D, Groner Y. Runx3 prevents spontaneous colitis by directing the differentiation of anti-inflammatory mononuclear phagocytes. PLoS One. 2020 May 26;15(5):e023304
51. Dicken J, Mildner A, Leshkowitz D, Touw IP, Hantisteanu S, Jung S, Groner Y. Transcriptional reprogramming of CD11b+Esam(hi) dendritic cell identity and function by loss of Runx3. PLoS One. 2013 Oct 15;8(10):e77490.
52. Puig-Kröger A, Domínguez-Soto A, Martínez-Muñoz L, Serrano-Gómez D, Lopez-Bravo M, Sierra-Filardi E, Fernández-Ruiz E, Ruiz-Velasco N, Ardavín C, Groner Y, Tandon N, Corbí AL, Vega MA. RUNX3 negatively regulates CD36 expression in myeloid cell lines. J Immunol. 2006 Aug 15;177(4):2107-14. doi: 10.4049/jimmunol.177.4.2107. PMID: 16887969.
53. Bosteels C, Neyt K, Vanheerswynghels M, van Helden MJ, Sichien D, Debeuf N, De Prijck S, Bosteels V, Vandamme N, Martens L, Saeys Y, Louagie E, Lesage M, Williams DL, Tang SC, Mayer JU, Ronchese F, Scott CL, Hammad H, Guilliams M, Lambrecht BN. Inflammatory Type 2 cDCs Acquire Features of cDC1s and Macrophages to Orchestrate Immunity to Respiratory Virus Infection. Immunity. 2020 Jun 16;52(6):1039-1056.e9. doi: 10.1016/j.immuni.2020.04.005. Epub 2020 May 8. PMID: 32392463; PMCID: PMC7207120.
54. Fasnacht N, Huang HY, Koch U, Favre S, Auderset F, Chai Q, Onder L, Kallert S, Pinschewer DD, MacDonald HR, Tacchini-Cottier F, Ludewig B, Luther SA, Radtke F. Specific fibroblastic niches in secondary lymphoid organs orchestrate distinct Notch-regulated immune responses. J Exp Med. 2014 Oct 20;211(11):2265-79. doi: 10.1084/jem.20132528. Epub 2014 Oct 13. PMID: 25311507; PMCID: PMC4203954.
55. Briseño CG, Satpathy AT, Davidson JT 4th, Ferris ST, Durai V, Bagadia P, O'Connor KW, Theisen DJ, Murphy TL, Murphy KM. Notch2-dependent DC2s mediate splenic germinal center responses. Proc Natl Acad Sci U S A. 2018 Oct 16;115(42):10726-10731.
56. Kirkling ME, Cytlak U, Lau CM, Lewis KL, Resteu A, Khodadadi-Jamayran A, Siebel CW, Salmon H, Merad M, Tsirigos A, Collin M, Bigley V, Reizis B. Notch Signaling Facilitates In Vitro Generation of Cross-Presenting Classical Dendritic Cells. Cell Rep. 2018

57. Fujita K, Chakarov S, Kobayashi T, Sakamoto K, Voisin B, Duan K, Nakagawa T, Horiuchi K, Amagai M, Ginhoux F, Nagao K. Cell-autonomous FLT3L shedding via ADAM10 mediates conventional dendritic cell development in mouse spleen. Proc Natl Acad Sci U S A. 2019 Jul 16;116(29):14714-14723. doi: 10.1073/pnas.1818907116. Epub 2019 Jul 1. PMID: 31262819; PMCID: PMC6642353.
58. Korenfeld D, Gorvel L, Munk A, Man J, Schaffer A, Tung T, Mann C, Klechevsky E. A type of human skin dendritic cell marked by CD5 is associated with the development of inflammatory skin disease. JCI Insight. 2017 Sep 21;2(18):e96101. doi: 10.1172/jci.insight.96101. PMID: 28931765; PMCID: PMC5621884.
59. Van Gassen S, Callebaut B, Van Helden MJ, Lambrecht BN, Demeester P, Dhaene T, Saeys Y. FlowSOM: Using self-organizing maps for visualization and interpretation of cytometry data. Cytometry A. 2015 Jul;87(7):636-45.
60. Jimenez-Dalmaroni MJ, Xiao N, Corper AL, Verdino P, Ainge GD, Larsen DS, Painter GF, Rudd PM, Dwek RA, Hoebe K, Beutler B, Wilson IA. Soluble CD36 ectodomain binds negatively charged diacylglycerol ligands and acts as a co-receptor for TLR2. PLoS One. 2009 Oct 22;4(10):e7411. doi: 10.1371/journal.pone.0007411. PMID: 19847289; PMCID: PMC2760212.
61. Kasper M, Heming M, Schafflick D, et al. Intraocular dendritic cells characterize HLA-B27-associated acute anterior uveitis. Elife. 2021;10:e67396. Published 2021 Nov 16. doi:10.7554/eLife.67396
62. Heger L, Balk S, Lühr JJ, Heidkamp GF, Lehmann CHK, Hatscher L, Purbojo A, Hartmann A, Garcia-Martin F, Nishimura SI, Cesnjevar R, Nimmerjahn F, Dudziak D. CLEC10A Is a Specific Marker for Human CD1c+ Dendritic Cells and Enhances Their Toll-Like Receptor 7/8-Induced Cytokine Secretion. Front Immunol. 2018 Apr 27;9:744. doi: 10.3389/fimmu.2018.00744. PMID: 29755453; PMCID: PMC5934495.
63. Kuiper JJW, Verhagen FH, Hiddingh S, Wennink RAW, Hansen AM, Casey KA, Hoefer IE, Haitjema S, Drylewicz J, Yakin M, Sen HN, Radstake TRDJ, de Boer JH. A serum protein network early predicts the need for systemic immunomodulatory therapy in non-infectious uveitis. Ophthalmol Sci. Published May 31, 2022. DOI: https://doi.org/10.1016/j.xops.2022.100175
64. Obermoser G, Pascual V. The interferon-alpha signature of systemic lupus erythematosus. Lupus. 2010 Aug;19(9):1012-9.
65. Touhami S, Diwo E, Sève P, Trad S, Bielefeld P, Sène D, Abad S, Brézin A, Quartier P, Koné Paut I, Weber M, Chiquet C, Errera MH, Sellam J, Cacoub P, Kaplanski G, Kodjikian L, Bodaghi B, Saadoun D. Expert opinion on the use of biological therapy in non-infectious uveitis. Expert Opin Biol Ther. 2019 May;19(5):477-490. doi: 10.1080/14712598.2019.1595578. Epub 2019 Apr 16. PMID: 30888881.
66. Horai R, Zárate-Bladés CR, Dillenburg-Pilla P, Chen J, Kielczewski JL, Silver PB, Jittayasothorn Y, Chan CC, Yamane H, Honda K, Caspi RR. Microbiota-Dependent Activation of an Autoreactive T Cell Receptor Provokes Autoimmunity in an Immunologically Privileged Site. Immunity. 2015 Aug 18;43(2):343-53. doi: 10.1016/j.immuni.2015.07.014. PMID: 26287682; PMCID: PMC4544742.
67. Ko HJ, Hong SW, Verma R, Jung J, Lee M, Kim N, Kim D, Surh CD, Kim KS, Rudra D, Im SH. Dietary Glucose Consumption Promotes RALDH Activity in Small Intestinal CD103+CD11b+ Dendritic Cells. Front Immunol. 2020 Aug 11;11:1897.
68. Croxford AL, Lanzinger M, Hartmann FJ, Schreiner B, Mair F, Pelczar P, Clausen BE, Jung S, Greter M, Becher B. The Cytokine GM-CSF Drives the Inflammatory Signature of CCR2+ Monocytes and Licenses Autoimmunity. Immunity. 2015 Sep 15;43(3):502-14.
69. Bing SJ, Silver PB, Jittayasothorn Y, Mattapallil MJ, Chan CC, Horai R, Caspi RR. Autoimmunity to neuroretina in the concurrent absence of IFN-γ and IL-17A is mediated by a GM-CSF-driven eosinophilic inflammation. J Autoimmun. 2020 Nov;114:102507.

Competing interests: Authors declare that they have no competing interests

Figure 1.

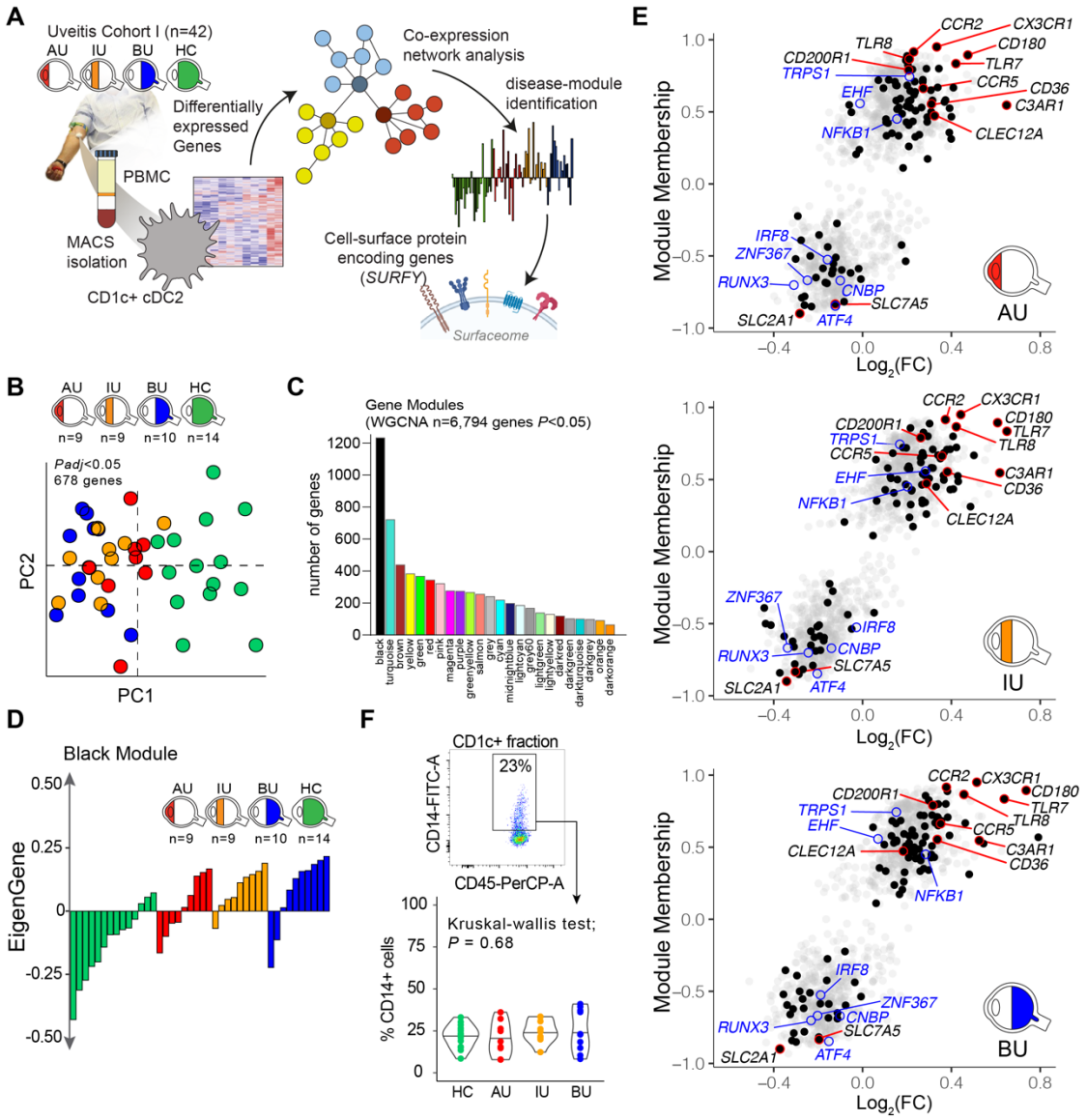
A
Uveitis Cohort I (n=42)
AU IU BU HC
Differentially expressed Genes
PBMC
MACS isolation
CD1c+ cDC2
Co-expression network analysis
disease-module identification
Cell-surface protein encoding genes (SURFY)
Surfaceome
B
AU IU BU HC
n=9 n=9 n=10 n=14
Padj<0.05
678 genes
PC2
PC1
C
Gene Modules
(WGCNA n=6,794 genes P<0.05)
number of genes
D
Black Module
EigenGene
F
CD1c+ fraction
23%
CD14-FITC-A
CD45-PerCP-A
Kruskal-wallis test;
P = 0.68
% CD14+ cells
HC AU IU BU
E
Module Membership
Log2(FC)
AU
IU
BU
CCR2
CX3CR1
CD180
TLR7
TLR8
CD200R1
TRPS1
EHF
CCR5
CD36
C3AR1
NFKB1
CLEC12A
IRF8
ZNF367
RUNX3
CNBP
SLC7A5
SLC2A1
ATF4

Figure 2.

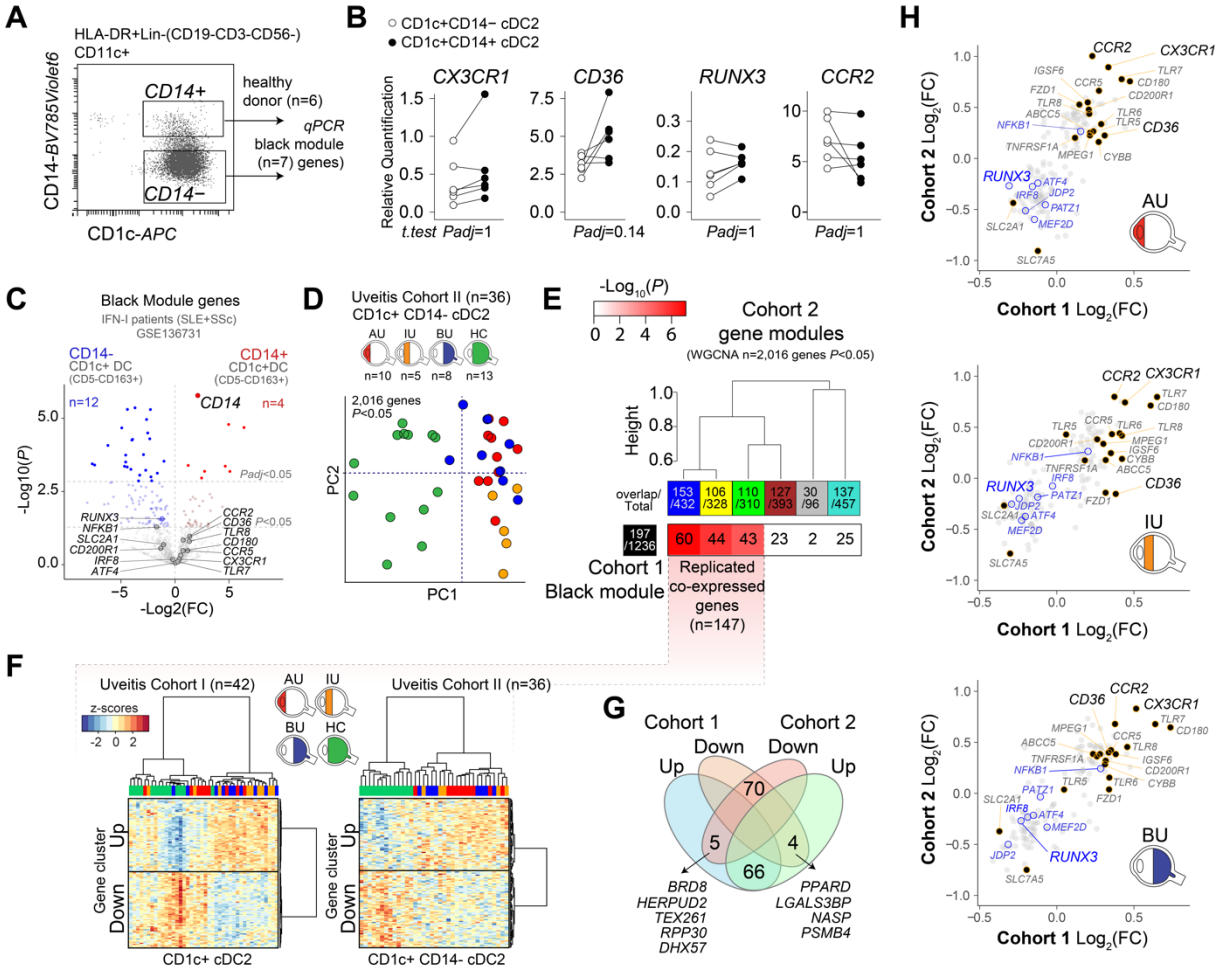
A
HLA-DR+Lin-(CD19-CD3-CD56-)
CD11c+
CD14+
CD14−
healthy donor (n=6)
qPCR
black module (n=7) genes)
CD14-BV785Violet6
CD1c-APC
B
CD1c+CD14− cDC2
CD1c+CD14+ cDC2
Relative Quantification
CX3CR1
CD36
RUNX3
CCR2
t.test Padj=1
Padj=0.14
Padj=1
Padj=1
C
Black Module genes
IFN-I patients (SLE+SSc)
GSE136731
CD14- CD1c+ DC (CD5-CD163+)
CD14+ CD1c+DC (CD5-CD163+)
n=12
n=4
CD14
Padj<0.05
P<0.05
-Log10(P)
-Log2(FC)
D
Uveitis Cohort II (n=36)
CD1c+ CD14- cDC2
AU IU BU HC
n=10 n=5 n=8 n=13
2,016 genes P<0.05
PC2
PC1
E
-Log10(P)
Cohort 2 gene modules
(WGCNA n=2,016 genes P<0.05)
Height
overlap/ Total
153 /432
106 /328
110 /310
127 /393
30 /96
137 /457
197 /1236
60 44 43 23 2 25
Cohort 1 Black module
Replicated co-expressed genes (n=147)
F
Uveitis Cohort I (n=42)
Uveitis Cohort II (n=36)
z-scores
Gene cluster
Up
Down
CD1c+ cDC2
CD1c+ CD14- cDC2
G
Cohort 1
Cohort 2
Up
Down
70
5
4
66
BRD8
HERPUD2
TEX261
RPP30
DHX57
PPARD
LGALS3BP
NASP
PSMB4
H
Cohort 2 Log2(FC)
Cohort 1 Log2(FC)
AU
IU
BU

Figure 3.

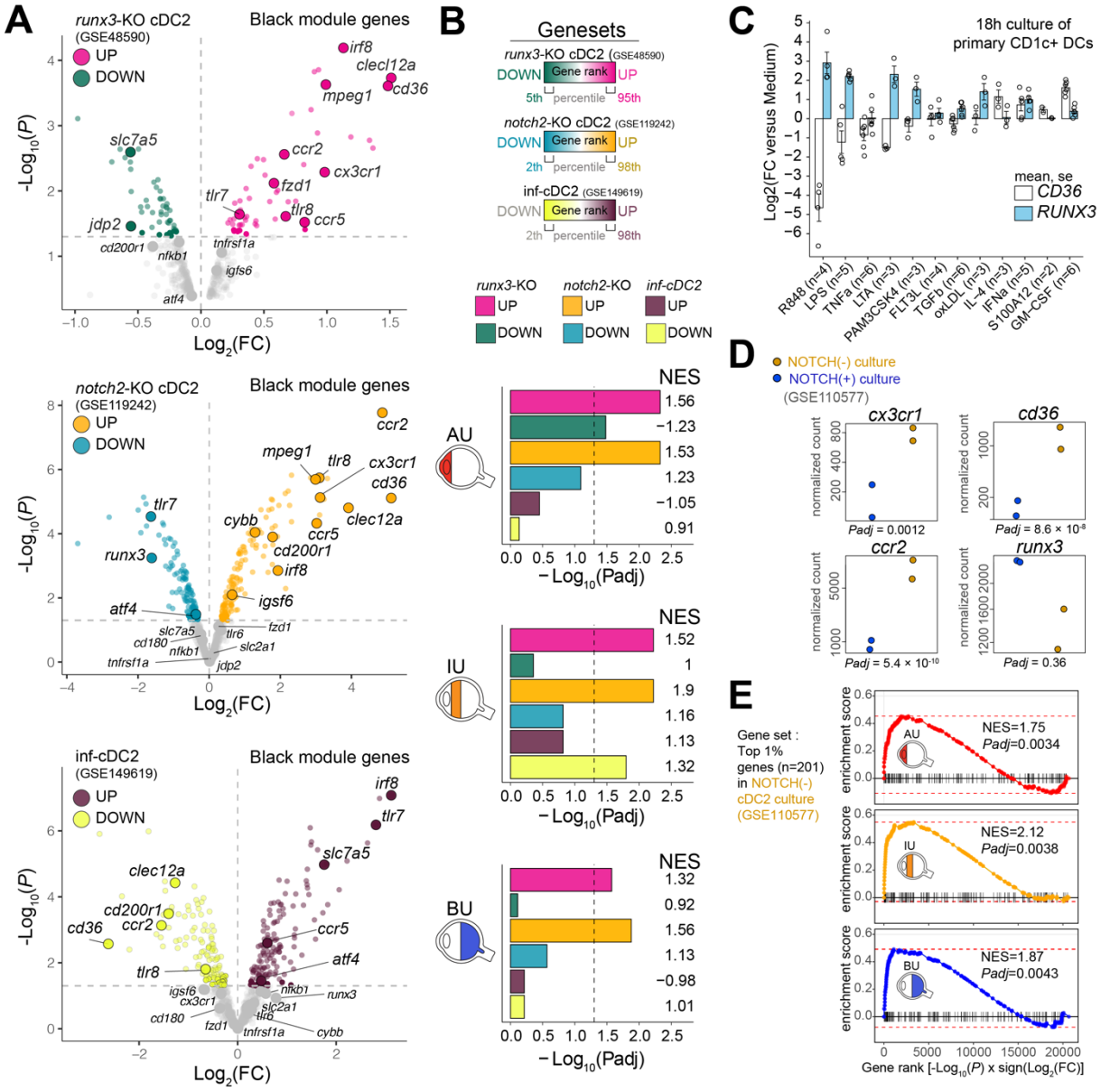
A
runx3-KO cDC2
(GSE48590)
UP
DOWN
Black module genes
irf8
clecl12a
cd36
mpeg1
slc7a5
ccr2
cx3cr1
fzd1
tlr7
tlr8
ccr5
jdp2
cd200r1
nfkb1
tnfrsf1a
igfs6
atf4
-Log10(P)
Log2(FC)
notch2-KO cDC2
(GSE119242)
UP
DOWN
Black module genes
ccr2
mpeg1
tlr8
cx3cr1
cd36
tlr7
cybb
clec12a
ccr5
runx3
cd200r1
irf8
igsf6
atf4
slc7a5
fzd1
cd180
tlr6
nfkb1
slc2a1
tnfrsf1a
jdp2
inf-cDC2
(GSE149619)
UP
DOWN
Black module genes
irf8
tlr7
slc7a5
clec12a
cd200r1
cd36
ccr2
ccr5
atf4
tlr8
igsf6
nfkb1
runx3
cx3cr1
slc2a1
cd180
tlr6
fzd1
tnfrsf1a
cybb
B
Genesets
runx3-KO cDC2 (GSE48590)
DOWN
Gene rank
UP
5th
percentile
95th
notch2-KO cDC2 (GSE119242)
DOWN
Gene rank
UP
2th
percentile
98th
inf-cDC2 (GSE149619)
DOWN
Gene rank
UP
2th
percentile
98th
runx3-KO
UP
DOWN
notch2-KO
UP
DOWN
inf-cDC2
UP
DOWN
AU
NES
1.56
−1.23
1.53
1.23
−1.05
0.91
−Log10(Padj)
IU
NES
1.52
1
1.9
1.16
1.13
1.32
−Log10(Padj)
BU
NES
1.32
0.92
1.56
1.13
−0.98
1.01
−Log10(Padj)
C
18h culture of
primary CD1c+ DCs
Log2(FC versus Medium)
mean, se
CD36
RUNX3
R848 (n=4)
LPS (n=5)
TNFa (n=6)
LTA (n=3)
PAM3CSK4 (n=3)
FLT3L (n=4)
TGFb (n=6)
oxLDL (n=3)
IL-4 (n=3)
IFNa (n=5)
S100A12 (n=2)
GM-CSF (n=6)
D
NOTCH(-) culture
NOTCH(+) culture
(GSE110577)
cx3cr1
normalized count
Padj = 0.0012
cd36
Padj = 8.6 × 10-8
ccr2
Padj = 5.4 × 10-10
runx3
Padj = 0.36
E
Gene set :
Top 1%
genes (n=201)
in NOTCH(-)
cDC2 culture
(GSE110577)
enrichment score
AU
NES=1.75
Padj=0.0034
IU
NES=2.12
Padj=0.0038
BU
NES=1.87
Padj=0.0043
Gene rank [-Log10(P) x sign(Log2(FC)]

Figure 4.

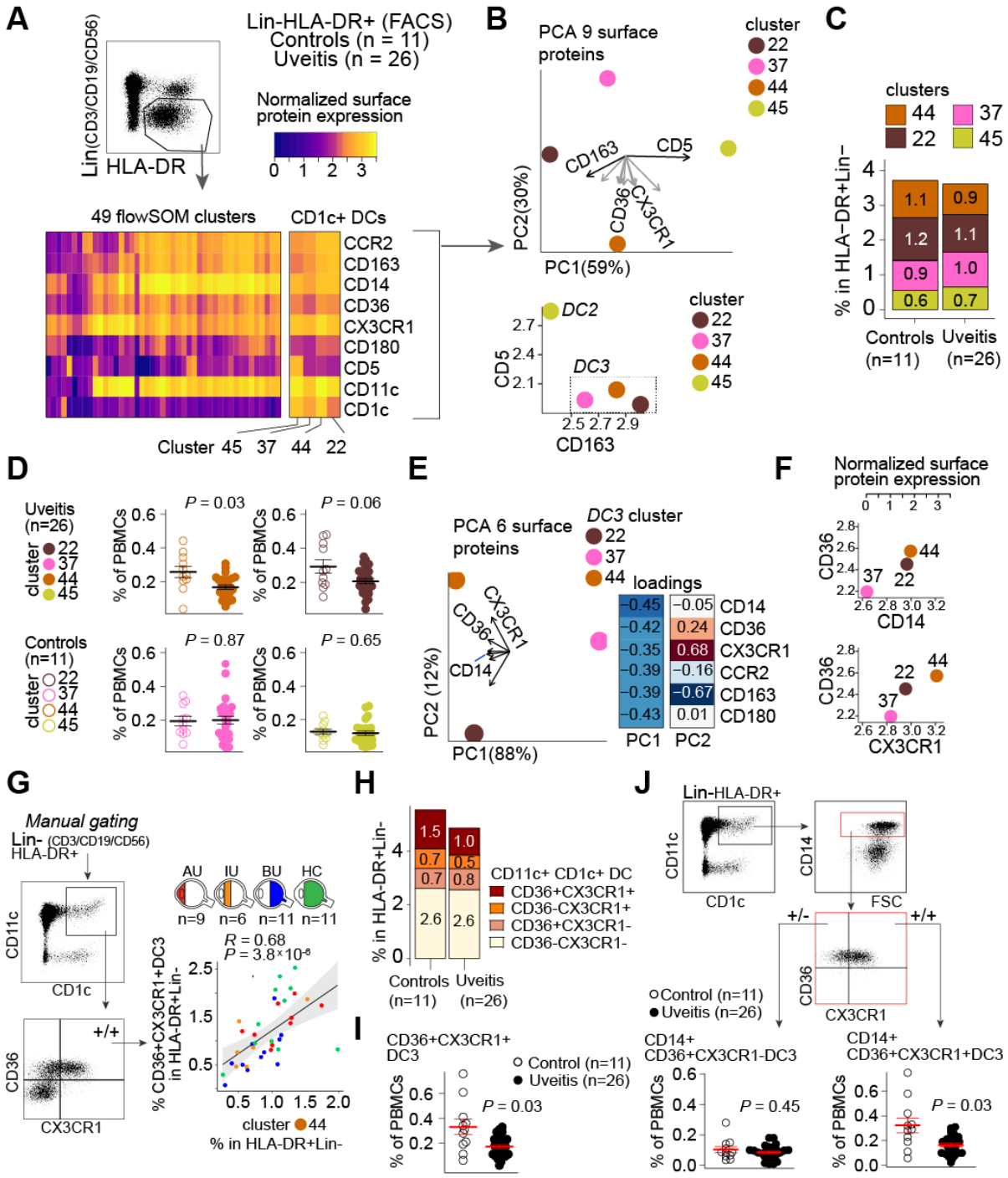
A
Lin-HLA-DR+ (FACS)
Controls (n = 11)
Uveitis (n = 26)
Lin(CD3/CD19/CD56)
HLA-DR
Normalized surface protein expression
0 1 2 3
49 flowSOM clusters
CD1c+ DCs
CCR2
CD163
CD14
CD36
CX3CR1
CD180
CD5
CD11c
CD1c
Cluster 45 37 44 22
B
PCA 9 surface proteins
cluster
22
37
44
45
CD163
CD5
CD36
CX3CR1
PC2(30%)
PC1(59%)
DC2
DC3
CD5
CD163
C
clusters
44 37
22 45
% in HLA−DR+Lin−
1.1 0.9
1.2 1.1
0.9 1.0
0.6 0.7
Controls (n=11)
Uveitis (n=26)
D
Uveitis (n=26)
Controls (n=11)
cluster 22 37 44 45
% of PBMCs
P = 0.03
P = 0.06
P = 0.87
P = 0.65
E
PCA 6 surface proteins
DC3 cluster
22
37
44
CX3CR1
CD36
CD14
PC2 (12%)
PC1(88%)
loadings
PC1 PC2
−0.45 −0.05 CD14
−0.42 0.24 CD36
−0.35 0.68 CX3CR1
−0.39 −0.16 CCR2
−0.39 −0.67 CD163
−0.43 0.01 CD180
F
Normalized surface protein expression
0 1 2 3
CD36
CD14
CX3CR1
37 22 44
G
Manual gating
Lin- (CD3/CD19/CD56)
HLA-DR+
CD11c
CD1c
CD36
CX3CR1
+/+
AU IU BU HC
n=9 n=6 n=11 n=11
R = 0.68
P = 3.8×10-6
% CD36+CX3CR1+DC3 in HLA-DR+Lin-
cluster 44
% in HLA-DR+Lin-
H
% in HLA-DR+Lin-
1.5 1.0
0.7 0.5
0.7 0.8
2.6 2.6
CD11c+ CD1c+ DC
CD36+CX3CR1+
CD36-CX3CR1+
CD36+CX3CR1-
CD36-CX3CR1-
Controls (n=11)
Uveitis (n=26)
I
CD36+CX3CR1+ DC3
Control (n=11)
Uveitis (n=26)
% of PBMCs
P = 0.03
J
Lin-HLA-DR+
CD11c
CD1c
CD14
FSC
+/-
+/+
CD36
CX3CR1
Control (n=11)
Uveitis (n=26)
CD14+ CD36+CX3CR1-DC3
CD14+ CD36+CX3CR1+DC3
% of PBMCs
P = 0.45
P = 0.03

Figure 5.

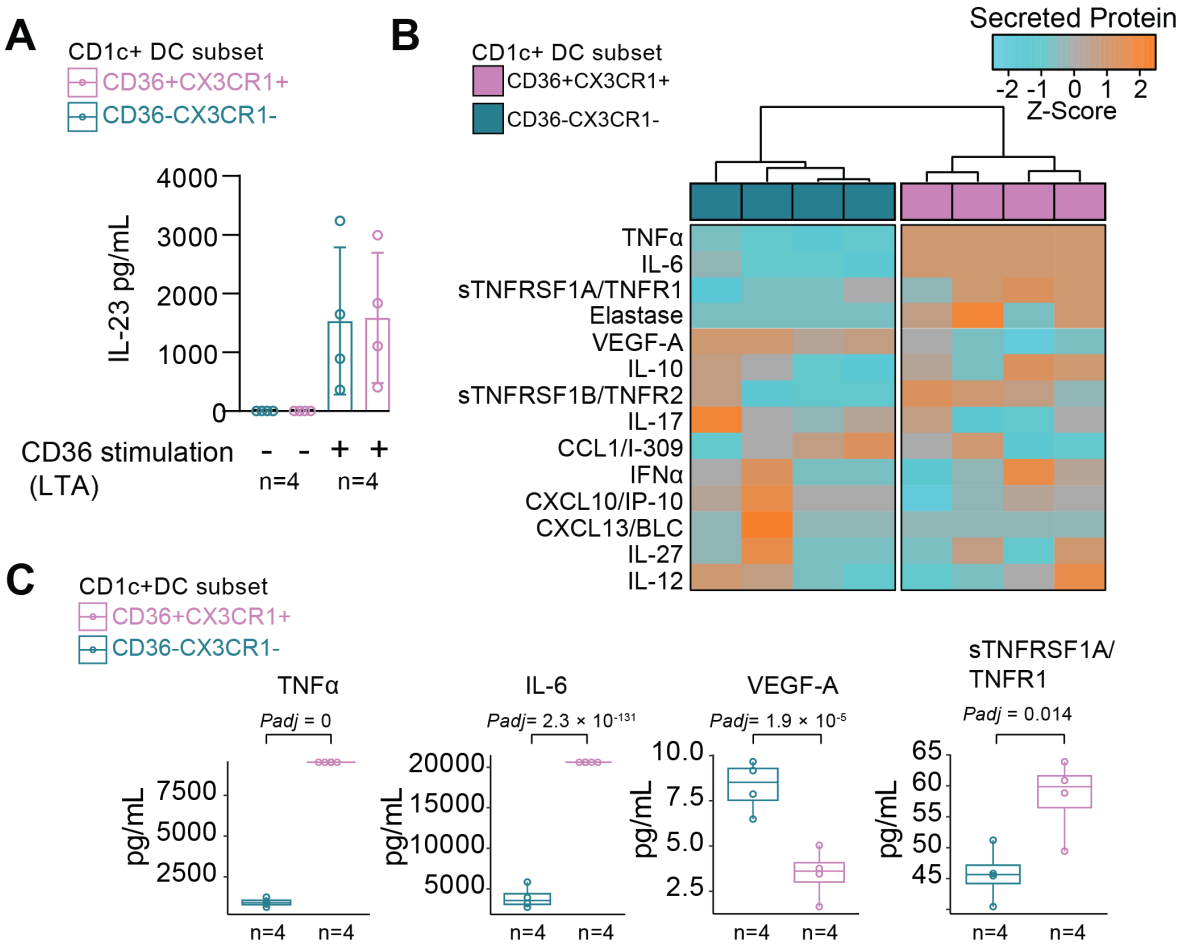
A
CD1c+ DC subset
CD36+CX3CR1+
CD36-CX3CR1-
IL-23 pg/mL
4000
3000
2000
1000
0
CD36 stimulation (LTA)
- - + +
n=4 n=4
B
CD1c+ DC subset
CD36+CX3CR1+
CD36-CX3CR1-
Secreted Protein
-2 -1 0 1 2
Z-Score
TNFα
IL-6
sTNFRSF1A/TNFR1
Elastase
VEGF-A
IL-10
sTNFRSF1B/TNFR2
IL-17
CCL1/I-309
IFNα
CXCL10/IP-10
CXCL13/BLC
IL-27
IL-12
C
CD1c+DC subset
CD36+CX3CR1+
CD36-CX3CR1-
TNFα
Padj = 0
IL-6
Padj= 2.3 × 10-131
VEGF-A
Padj= 1.9 × 10-5
sTNFRSF1A/ TNFR1
Padj = 0.014
pg/mL
n=4 n=4

Figure 6.

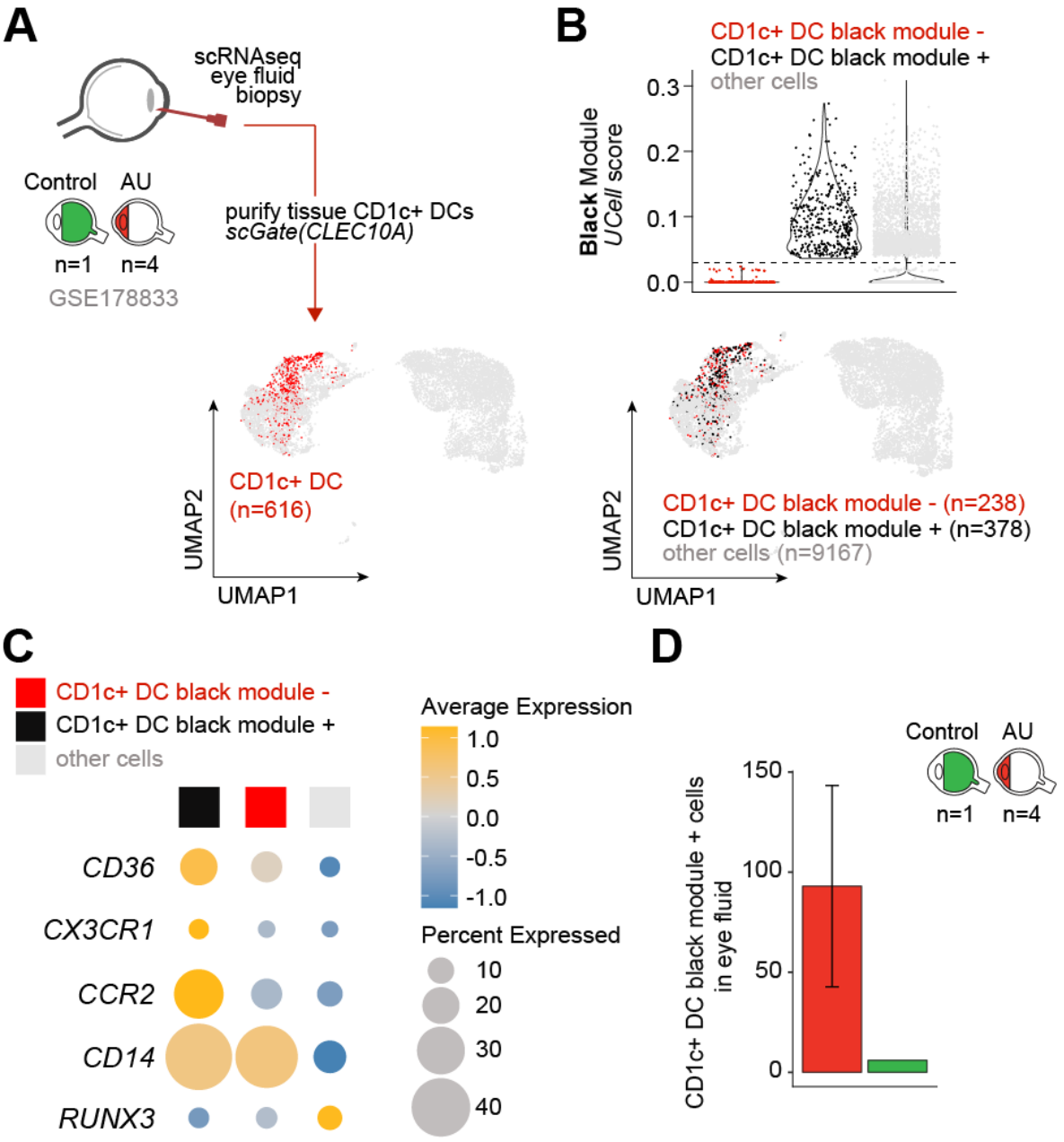
A
scRNAseq
eye fluid
biopsy
Control
AU
n=1
n=4
GSE178833
purify tissue CD1c+ DCs
scGate(CLEC10A)
CD1c+ DC
(n=616)
UMAP2
UMAP1
B
CD1c+ DC black module -
CD1c+ DC black module +
other cells
Black Module
UCell score
0.3
0.2
0.1
0.0
CD1c+ DC black module - (n=238)
CD1c+ DC black module + (n=378)
other cells (n=9167)
UMAP2
UMAP1
C
CD1c+ DC black module -
CD1c+ DC black module +
other cells
CD36
CX3CR1
CCR2
CD14
RUNX3
Average Expression
1.0
0.5
0.0
-0.5
-1.0
Percent Expressed
10
20
30
40
D
Control
AU
n=1
n=4
CD1c+ DC black module + cells
in eye fluid
150
100
50
0

Figure Legends:

Figure 1. A CD1c+ Dendritic cell (CD1c+ DC) transcriptional module is increased in expression in human non-infectious uveitis. A) Study design. CD1c+ DCs were purified from blood and subjected to RNA sequencing. Co-expression network analysis was used to identify gene modules associated with uveitis and focus on the surface-protein encoding genes (predicted by *SURFY*[46]) and their transcriptional regulators. **B**) Principal component analysis of the 678 differentially expressed genes (*Padj*<0.05) **C**) Number of genes for each of the 24 identified gene modules based on 6,794 uveitis-associated genes (*P*<0.05). **D**) The *EigenGene* values for the black module (y-axis) for each sample of cohort 1 (x-axis). **E**) The module membership (y-axis) and the (Log2) fold change in gene expression compared to healthy controls (x-axis) for genes in the black module in patients with AU (top), IU (middle), and BU (bottom). The 100 genes encoding surface proteins are indicated in black. Key transcription factors associated with functionally distinct CD1c+ DC subsets[47] are indicated in blue. **F**) The percentage of CD14-positive cells in the CD19(-) CD304(-) CD1c(+) cell fractions used for RNA sequencing. AU; Anterior uveitis. IU; Intermediate uveitis. BU; Birdshot uveitis.

Figure 2. The CD1c+ DC transcriptional signature of non-infectious uveitis is independent of CD14 cell surface expression. A) Gating strategy to sort CD14+ and CD14- CD1c+ DCs from healthy donors. **B**) RT-qPCR results for a panel of genes of the black module in the sorted CD14+ and CD14- CD1c+ DC fractions in *a*. *Padj* = adjusted *P* values from t.test (Bonferroni) corrected for 7 genes (see also **Figure 2 – Supplement 1B**). **C**) Volcano plot showing differential expression analysis (DESeq2 output) for black module genes in CD14+ versus CD14- CD1c+ DCs purified from SLE and SSc patients (GSE136731). **D**) Principal component analysis of the 2,016 uveitis-associated genes (*P*<0.05) in 36 patients and control samples of cohort 2. **E**) Cross-tabulation of the preservation of co-expressed genes from the black module in the second cohort. Each row and each column are labeled by the corresponding module color and the total number of genes in the module. The numbers represent the counts of genes in the intersection of the black module and modules identified in the second cohort. *P* value is from Fisher's exact test. **F**) Heatmaps of the 147 replicated co-expressed genes (rows) for samples (columns) from cohort 1 and cohort 2. **G**) Venn diagram of the upregulated and downregulated genes (clusters shown in **F**) from cohort 1 and 2. **H**) The (Log2) fold change in gene expression compared to healthy controls (x-axis) for all 147 replicated genes in patients with AU, IU, AND BU. Genes encoding surface proteins are indicated in black/grey. Key transcription factors are indicated in blue. AU; Anterior uveitis. IU; Intermediate uveitis. BU; Birdshot uveitis.

Figure 3. Aberrant NOTCH2-RUNX3 signaling recapitulates the transcriptional module of CD1c+ DCs in non-infectious uveitis. A) Volcano plot for the expression of genes of the black module in cDC2s of *runx3*-KO mice (GSE48590), *notch2*-KO mice (GSE119242), and inflammatory [inf-]cDC2s (GSE149619). Up-regulated genes and down-regulated genes for each condition are indicated for each condition; grey dots denote the genes with no significant change in expression. Key genes identified in the uveitis cohorts (see **Figure 2H**) are labeled. **B**) Results from gene-set enrichment analysis for ranked transcriptome (using 20,668 genes with *baseMean*>4) for AU, IU, and BU patients. The top or bottom percentiles of the ranked [$-\log_{10}(P) \times \text{sign}(\log_2(FC))$] genes from *runx3*-KO cDC2s, *notch2*-KO cDC2s, and inf-cDC2s (see *a*) were used as gene sets. Normalized enrichment scores (NES) and *P* values for each gene set is indicated. The dotted lines indicate *Padj* = 0.05. **C**) Gene expression (mean [SEM]) for *RUNX3* and *CD36* in primary human CD1c+ DCs from healthy donors stimulated overnight. Each dot represents a single donor used in the experiment. **D**) Normalized counts (and adjusted *P* values from *DESeq2*) for *cx3cr1*, *ccr2*, *cd36*, and *runx3* from cDC2s (GSE110577) generated from murine bone marrow cells and OP-9 with (in blue) or without (in ochre) Notch ligand Delta-like 1 (DLL1). **E**) Gene set enrichment analysis similar to ***b***, using

the top 1%, (n=201) genes associated with the NOTCH-negative condition in *d* as the gene set. AU = Anterior uveitis. IU = Intermediate uveitis. BU = Birdshot uveitis. R848 = Resiquimod, LTA = Lipoteichoic acid, LPS = Lipopolysaccharides, Pam3CSK4 = Pam3CysSerLys4, OxLDL = Oxidized low-density lipoprotein, IFNα = Interferon alpha, TGFβ = transforming growth factor beta. FLT3L = FMS-like tyrosine kinase 3 ligand, TNFα = tumor necrosis factor alpha, S100A12 = S100 calcium-binding protein A12, IL-4 = interleukin 4, GM-CSF = Granulocyte-macrophage colony-stimulating factor.

Figure 4. A CD36+CX3CR1+ subpopulation of CD14+ DC3s is decreased in blood of patients with non-infectious uveitis. A) Heatmap of the surface protein expression for 49 flowSOM clusters of flow-cytometry analysis of PBMC samples from 26 patients and 11 controls. The four CD1c+ (CD3-CD19-CD56-HLA-DR+CD11c+) DC clusters identified (cluster 22, 37, 44, and 45) are shown (detailed heatmap in **Figure 4 – Supplement 1A**). **B**) PCA biplot of the surface protein expression for clusters 22, 37, 44, and 45 identified in *a* (**Figure 4 – Supplement 1B)**. bottom: biplot of the normalized surface expression of CD5 and CD163 for the 4 CD1c+ DC clusters. **C**) The proportion of the 4 CD1c+ DC cluster in the HLA-DR+Lin-(CD3-CD19-CD56) population in controls and patients. **D**) The frequency of the 4 CD1c+DC flowSOM clusters as percentage of PBMCs. *P* values from *Welch's t-test*. **E**) PCA biplot of the DC3 clusters 22, 37, and 44. Loadings for PC1 and PC2 are shown on the right. **F**) Biplots of the normalized surface expression of CD36, CD14, and CX3CR1 in the DC3 clusters 22, 37, and 44. **G**) Manual gating strategy of CD1c+ DC subsets based on CD36 and CX3CR1 and the correlation between CD36+CX3CR1+ CD1c+ DCs and the flowSOM cluster 44. *R* = Spearman correlation. Gray area represents 95% confidence interval of the linear regression line. **H**) The relative proportion of CD1c+ DC subsets based on CD36 and CX3CR1 in the HLA-DR+ Lin- gate. **I**) the frequency (%) of manually gated CD36+CX3CR1+ CD1c+ DCs, in PBMCs in uveitis cases and controls. *P* value from *Welch's t* test. **J**) Manual gating strategy and frequency (%) of CD14+CD1c+ DC3 subsets based on CD36 and CX3CR1. Details on manual gating strategy: see **Figure 4 – Supplement 2**. *P* values from *Welch's t* test.

Figure 5. CD36+CX3CR1+DC3s secrete high levels of cytokines implicated in non-infectious uveitis. A) The CD1c+ DC cells were FACS sorted into CD36+CX3CR1+ and CD36-CX3CR1- CD1c+ DCs (**Figure 5 – Supplement 1**). The concentration of IL-23 (ELISA) in supernatants of 18h cultured primary human CD1c+ DC subsets cells stimulated with lipoteichoic acid (LTA). **B**) Heatmap of the levels (Z-score) of 16 detected proteins in supernatants of 18h cultured LTA-stimulated primary human CD1c+ DC subsets cells using an in-house multiplex *Luminex* assay (**Supplementary File 1E**). **C**) Scatter plots with overlay boxplot with mean and interquartile range of the levels of secreted TNF-alpha, Interleukin (IL)-6, VEGF-A, and TNFR1 from the multiplex protein data in *d.* (*Padj* = *P* values from likelihood ratio test Bonferroni corrected for 16 detected proteins).

Figure 6. CD36+CX3CR1+DC3s infiltrate the inflamed eye during non-infectious uveitis. A) Single-cell RNA-sequencing (scRNAseq) analysis of eye fluid biopsies from non-infectious uveitis patients (AU) and control (n=5, *GSE178833*). UMAP projections of transcriptomic data from 616 CD1c+ DC cells (in red) identified by *scGate* analysis (using *CLEC10A* as tissue marker for CD1c+ DCs). **B**) Clustering of CD1c+ DCs identified in *a* based on the *UCell module score* for the black module gene signature (i.e., *UCell score* for genes with high *Module Membership* = -0.85< or >0.85, n=18 genes, **Supplementary File 1G**). **C**) Dot plot showing average expression (color-scaled) of key marker genes of the black module and *CD14* in each cluster determined in *B*. Dot size reflects the proportion of cells expressing the selected gene. **D**) Barplot showing the average number of CD36+CX3CR1+ DC3s in eye fluid biopsies of patients and the control analyzed by scRNAseq.

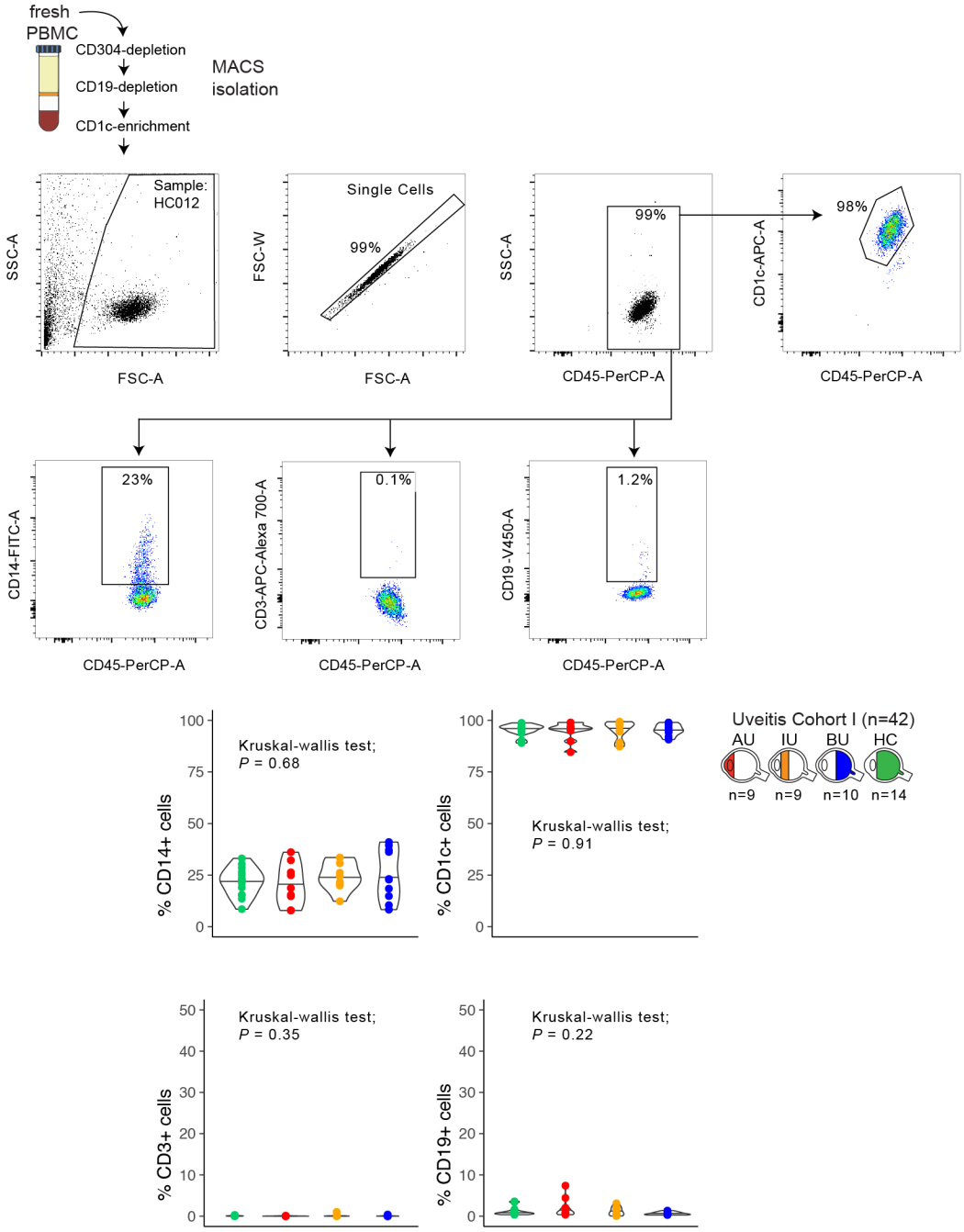

Figure 1 – Supplement 1. Purity check of cell fractions for RNA-sequencing in cohort I. Representative sample of flow cytometry gating of CD14+, CD19+, CD3+ and CD1c+ cell fractions in CD304-depleted, CD19-depleted and CD1c+ enriched MACS fractions from fresh peripheral blood mononuclear cells. Manual gating data for each individual sample is available via: https://doi.org/10.34894/9Q0FVO. The percentage of cells positive for each marker on the group levels between the disease groups is indicated in the bottom.

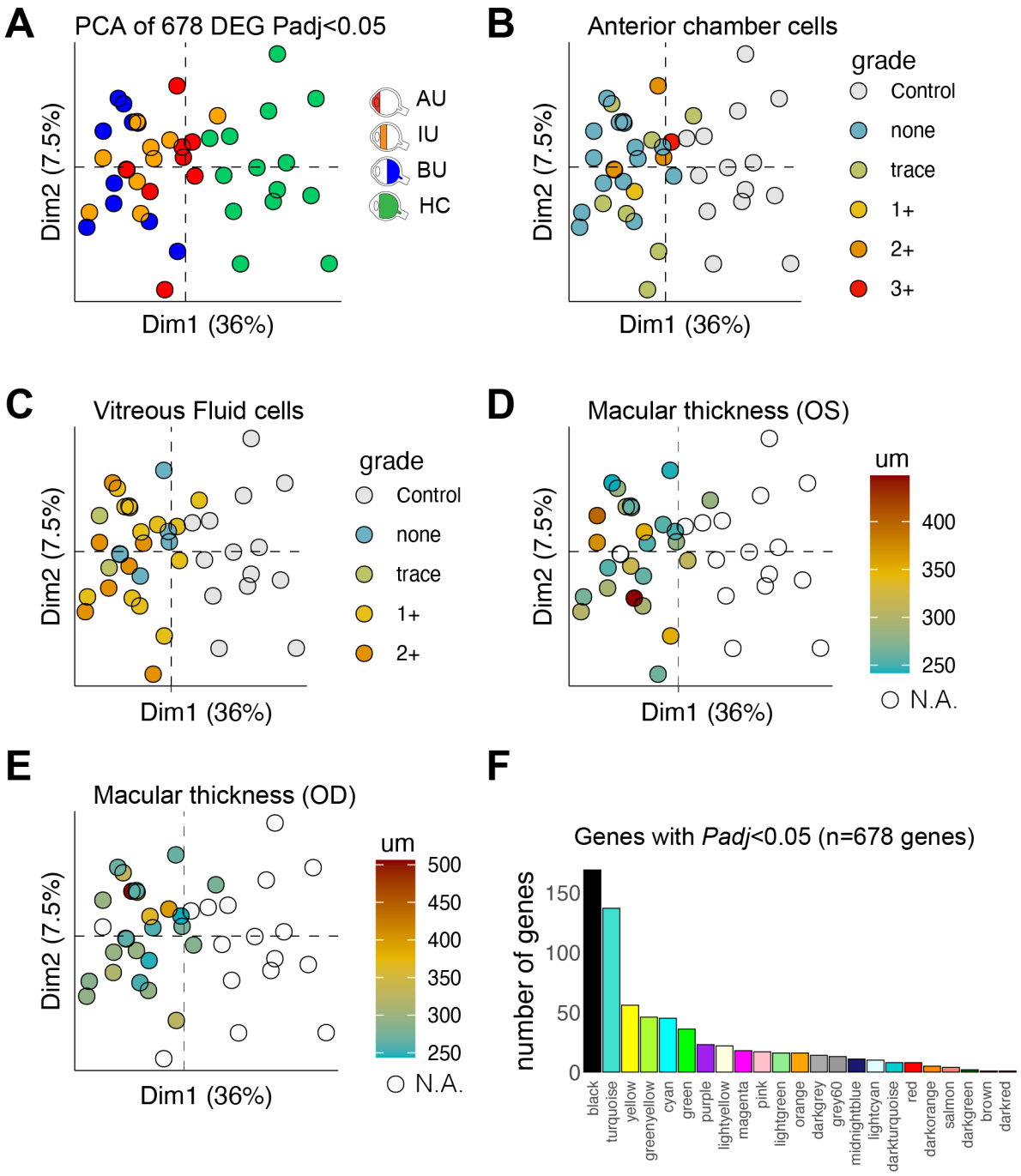

Figure 1 – Supplement 2. Clinical parameters of disease activity in non-infectious uveitis in cohort I. **A-E)** A PCA plot based on the 678 differentially expressed genes (*Padj*<0.05) as shown in Figure 1B (**A**) the anterior chamber cell grade (**B**), Vitreous fluid cell grade (**C**), macular thickness in the left (OS) eye as determined by optical coherence tomography (OCT) (**D**), and macular thickness in the right eye (OD) as determined by OCT (**E**) are shown. **F**) Number of genes for each of the 24 identified gene modules based on 678 differentially expressed genes (*Padj*<0.05).

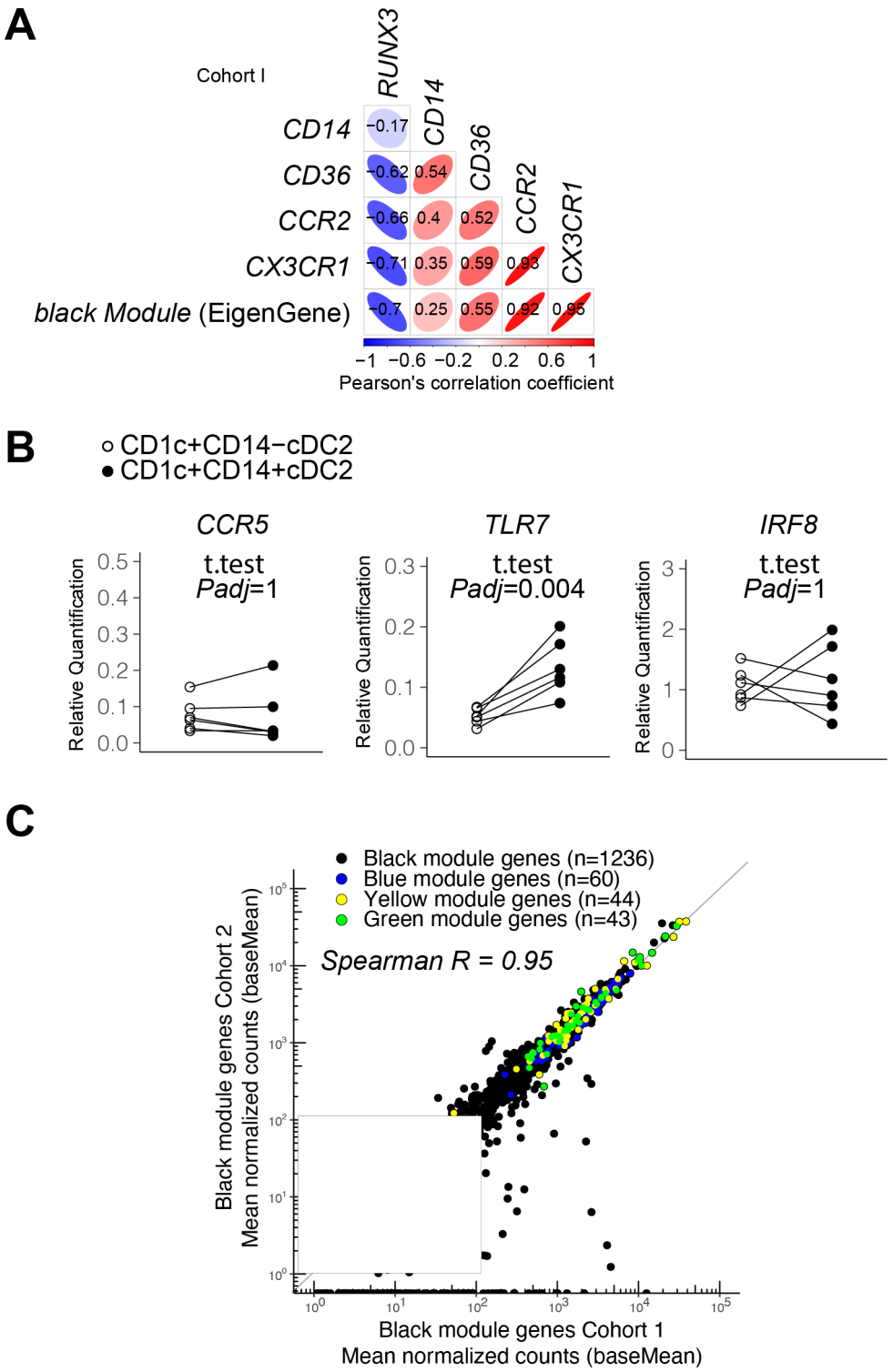

Figure 2 – Supplement 1. A) Correlation plot of the gene expression levels of CD14, CD36, CCR2, CX3CR1, and the *EigenGene* value of the black module. **B**) RT-qPCR results (supplement to ***Figure 2B***) for *CCR5*, *TLR7*, and *IRF8* from the black module in CD14+ and CD14- CD1c+ DCs. Padj = adjusted *P* values from t.test (Bonferroni) corrected for 7 genes. **C**) Correlation plot of the mean normalized count (*baseMean* from *DESeq2*) of the black module genes from cohort 1 and the 147 overlapping genes in the blue, yellow, and green module in cohort 2.

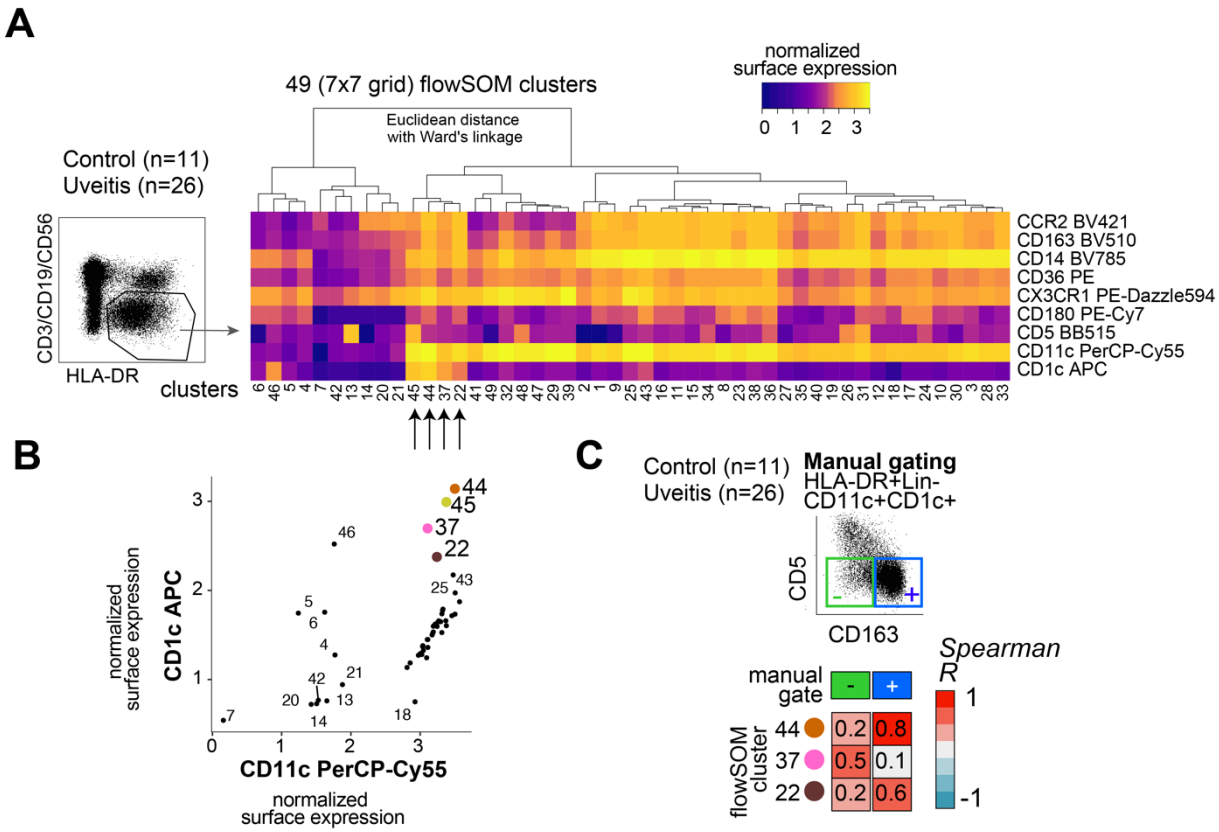

Figure 4 – Supplement 1. A) Heatmap of the surface protein expression for 49 flowSOM clusters of flow-cytometry analysis of PBMC samples from 26 patients and 11 controls. The four CD1c+ (CD3-CD19-CD56-HLA-DR+CD11c+) DC clusters identified (cluster 22, 37, 44, and 45) are highlighted. **B**) Biplot of the cell surface expression of CD1c and CD11c for the 49 flowSOM clusters in *a*. **C**) Correlation plot between manually gated CD5-CD163- DC3s and CD5-CD163+ DC3s and DC3 flowSOM clusters 22, 37, and 44.

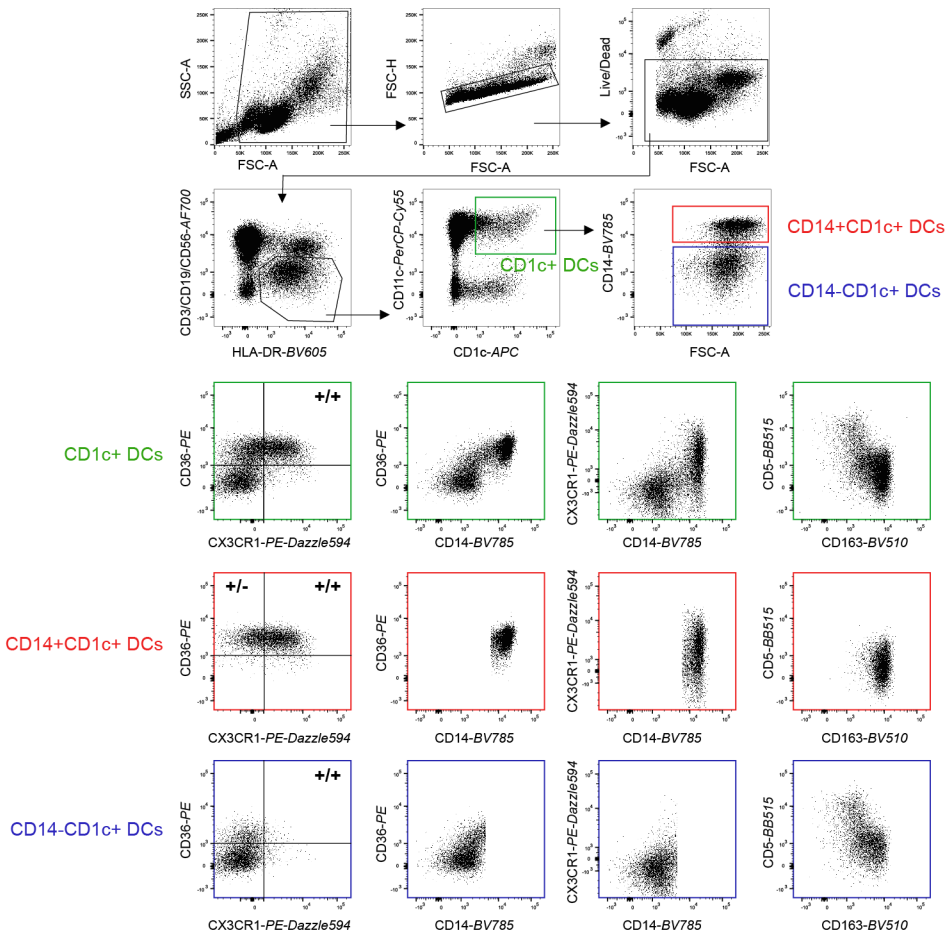

Figure 4 – Supplement 2. Representative sample of flow cytometry gating of CD14+ and CD14- fractions of CD1c+ DCs in peripheral blood for the panel used in Figure 4. Manual gating revealed that the CD14+ CD1c+ DCs (DC3s) can be further subdivided in a CD36+CX3CR1- and a CD36+ CX3CR1+ population.

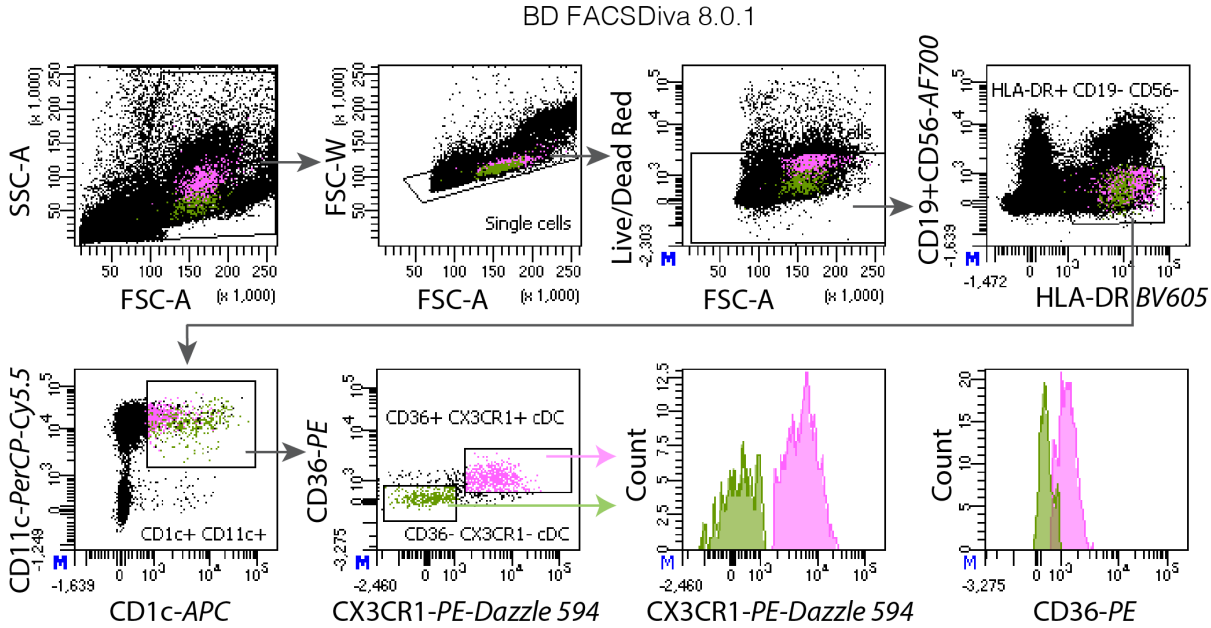

Tube: donor 1 Buffy

Population	#Events	%Parent	%Total
All Events	181,274	####	100.0
FCS/SSC	100,037	55.2	55.2
Single cells	94,165	94.1	51.9
Live cells	92,026	97.7	50.8
HLA-DR+ CD19- CD56-	20,907	22.7	11.5
CD1c+ CD11c+	1,135	5.4	0.6
CD36+ CX3CR1+ cDC	589	51.9	0.3
CD36- CX3CR1- cDC	345	30.4	0.2

Figure 5 – Supplement 1. Representative examples of fluorescent-activated cell sorting (FACS) of CD36+CX3CR1+ DC3s and CD36-CX3CR1- CD1c+ DCs used for the analysis in Figure 5A and 5B.

Table 1.

Discovery cohort	AU	IU	BU	HC	*P* value
N	9	9	10	14	Total=42
Male / Female	3/6	2/7	4/6	6/8	0.8790*
Age in years; mean ± SD	47. ± 17	39 ± 14	52 ± 13	39 ± 10	0.06***
Disease duration in years; median (range)	5.8 (0.1-39.3)	3.7 (0.2-20.0)	1.3 (0.2-15.1)	n.a.	0.14**
Replication cohort	AU	IU	BU	HC	*P* value
N	10	5	8	13	Total=36
Male / Female	2/8	3/2	5/3	5/8	0.26*
Age in years; mean ± SD	45 ± 16	30 ± 9	42 ± 10	42 ± 13	0.24***
Disease duration in years; median (range)	8.1 (0.2-22.3)	3.4 (0.4-14.1)	0.9 (0.2-19.9)	n.a.	0.36**

Table 1. Characteristics of the patients and controls from cohort 1 and cohort 2. Abbreviations: BU: Birdshot uveitis, AU: HLA-B27 associated anterior uveitis, HC: healthy control, IU: idiopathic intermediate uveitis, n.a.: not applicable, * Fisher's exact test, ** ANOVA,*** Kruskal-Wallis.

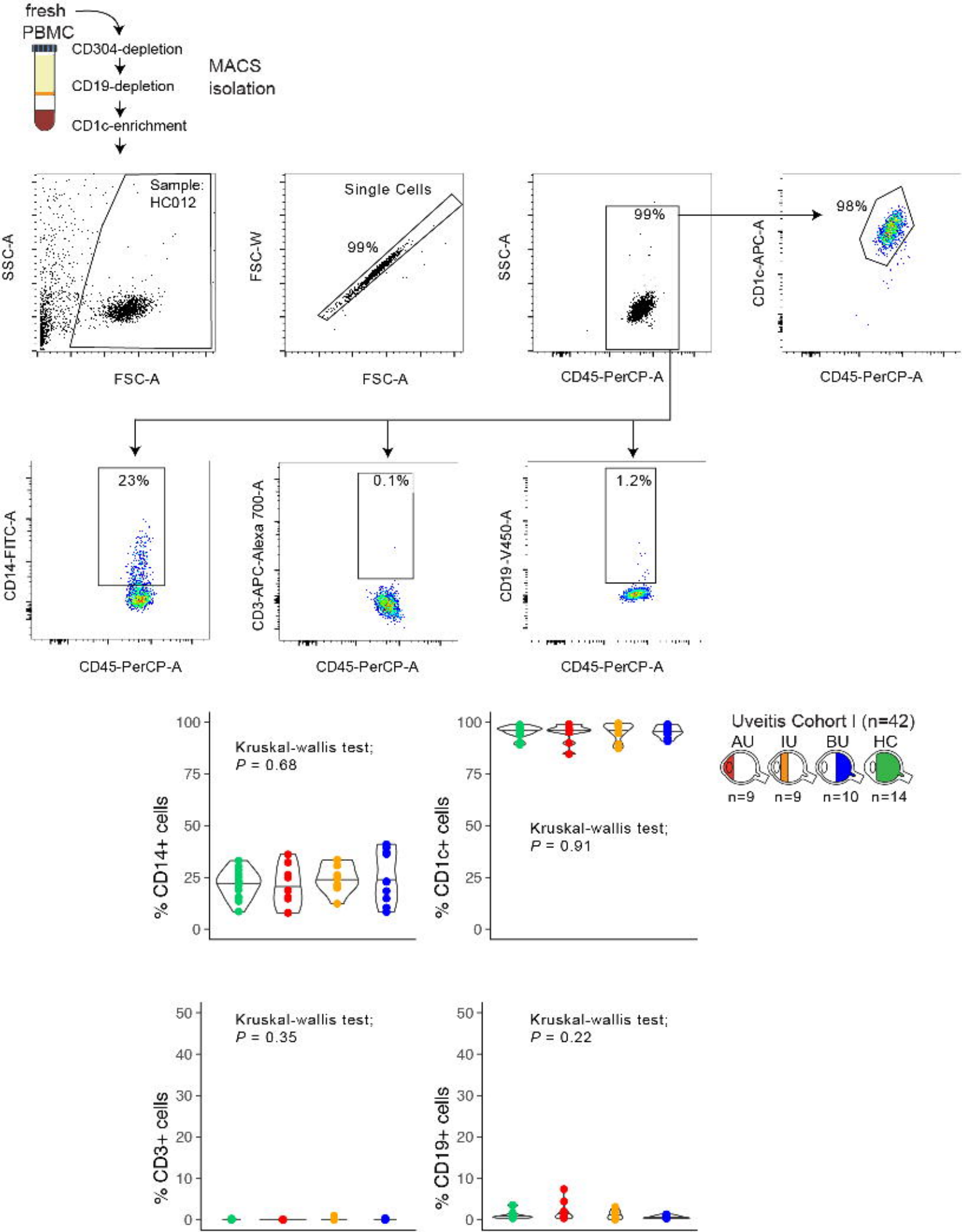
fresh PBMC
CD304-depletion
CD19-depletion
CD1c-enrichment
MACS isolation
Sample: HC012
SSC-A
FSC-A
Single Cells
99%
FSC-W
FSC-A
99%
SSC-A
CD45-PerCP-A
98%
CD1c-APC-A
CD45-PerCP-A
23%
CD14-FITC-A
CD45-PerCP-A
0.1%
CD3-APC-Alexa 700-A
CD45-PerCP-A
1.2%
CD19-V450-A
CD45-PerCP-A
Kruskal-wallis test; P = 0.68
% CD14+ cells
Kruskal-wallis test; P = 0.91
% CD1c+ cells
Uveitis Cohort I (n=42)
AU
IU
BU
HC
n=9
n=9
n=10
n=14
Kruskal-wallis test; P = 0.35
% CD3+ cells
Kruskal-wallis test; P = 0.22
% CD19+ cells

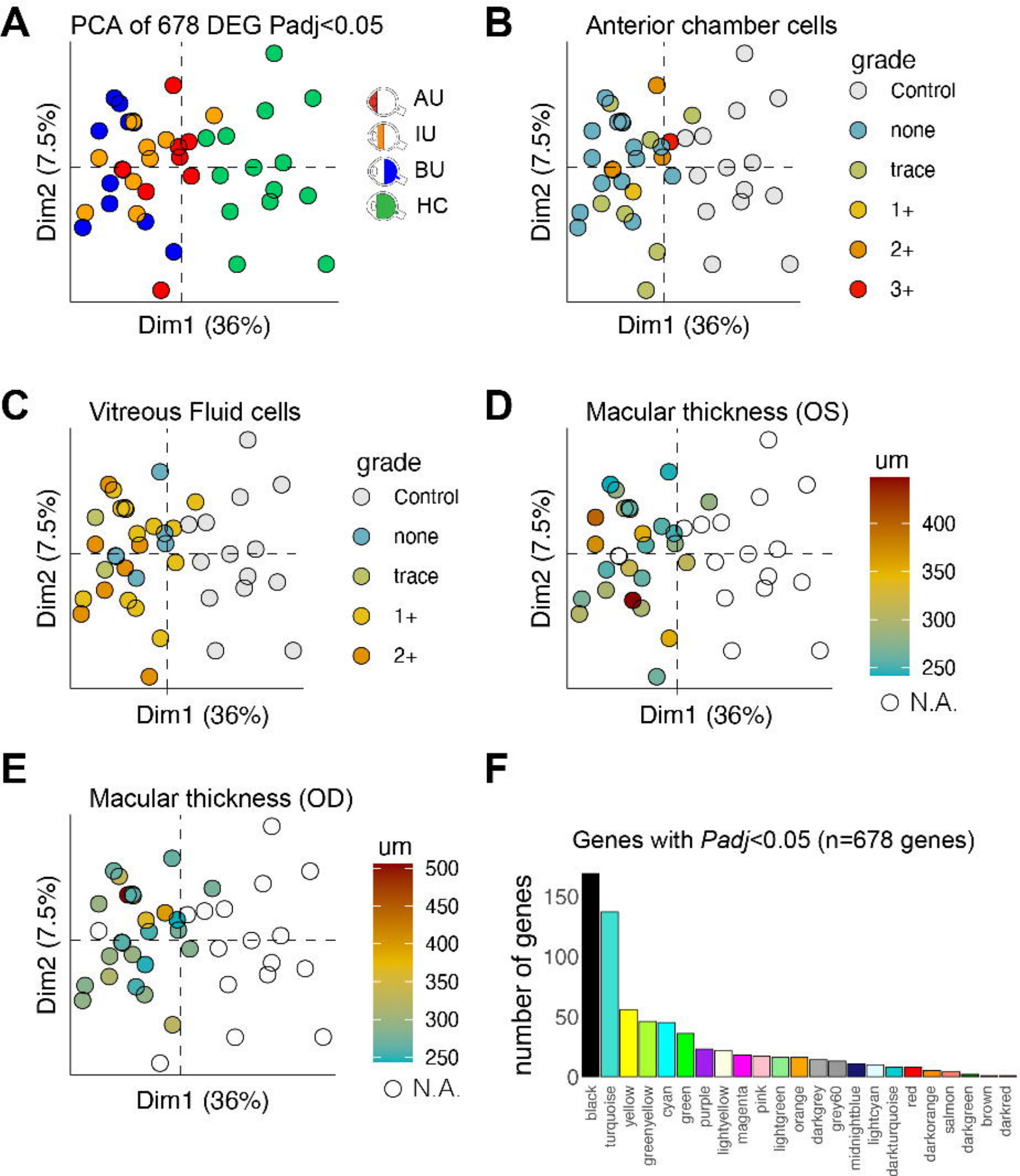
A
PCA of 678 DEG Padj<0.05
Dim2 (7.5%)
Dim1 (36%)
AU
IU
BU
HC
B
Anterior chamber cells
grade
Control
none
trace
1+
2+
3+
C
Vitreous Fluid cells
D
Macular thickness (OS)
um
400
350
300
250
N.A.
E
Macular thickness (OD)
500
450
F
Genes with Padj<0.05 (n=678 genes)
number of genes
150
100
50
0
black
turquoise
yellow
greenyellow
cyan
green
purple
lightyellow
magenta
pink
lightgreen
orange
darkgrey
grey60
midnightblue
lightcyan
darkturquoise
red
darkorange
salmon
darkgreen
brown
darkred

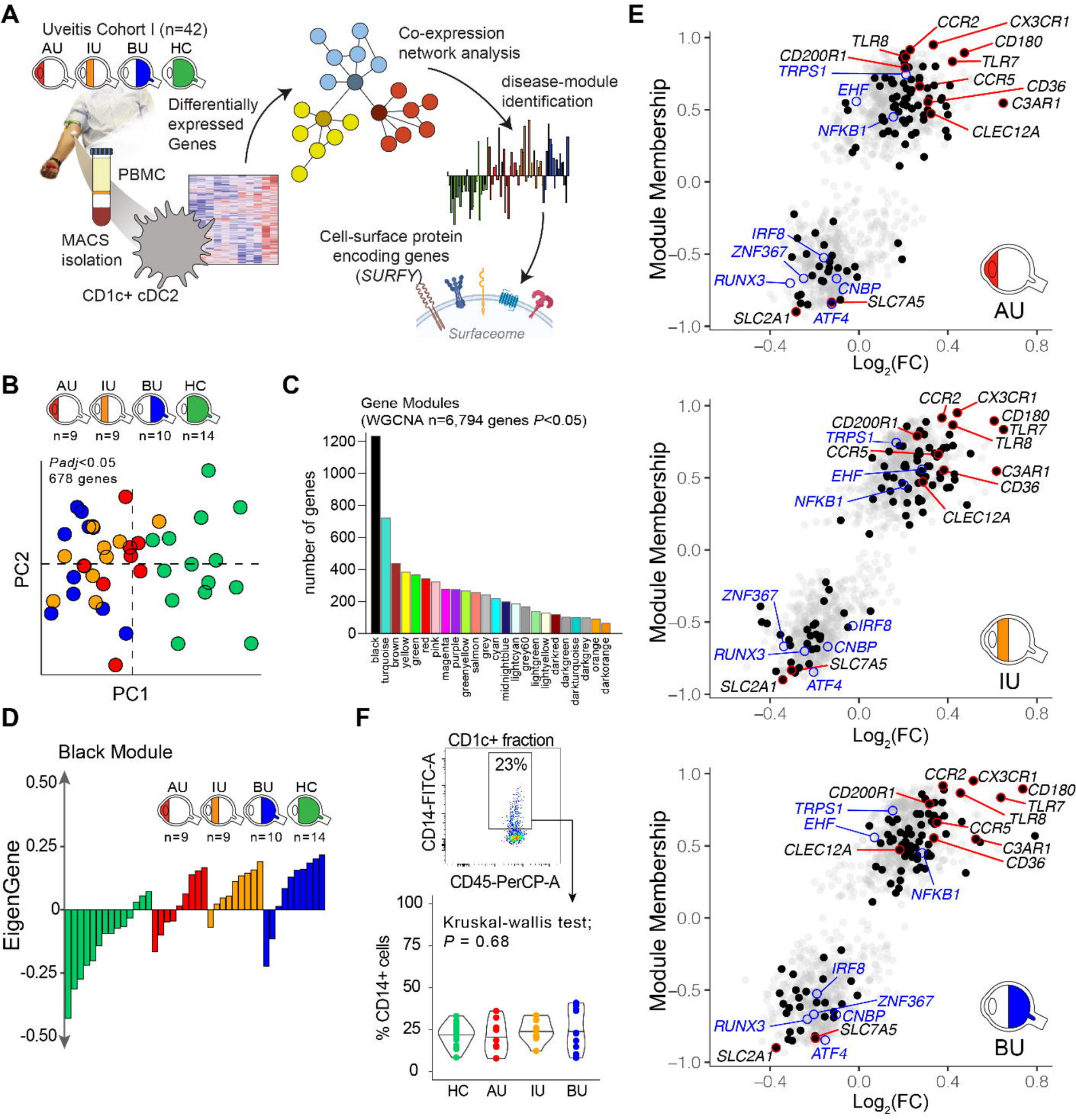
A
Uveitis Cohort I (n=42)
AU
IU
BU
HC
Differentially expressed Genes
PBMC
MACS isolation
CD1c+ cDC2
Co-expression network analysis
disease-module identification
Cell-surface protein encoding genes (SURFY)
Surfaceome
B
n=9
n=9
n=10
n=14
Padj<0.05
678 genes
PC2
PC1
C
Gene Modules
(WGCNA n=6,794 genes P<0.05)
number of genes
black
turquoise
brown
yellow
green
red
pink
magenta
purple
greenyellow
salmon
grey
cyan
midnightblue
lightcyan
grey60
lightgreen
lightyellow
darkred
darkgreen
darkturquoise
darkgrey
orange
darkorange
D
Black Module
EigenGene
F
CD1c+ fraction
23%
CD14-FITC-A
CD45-PerCP-A
Kruskal-wallis test;
P = 0.68
% CD14+ cells
HC
AU
IU
BU
E
Module Membership
Log2(FC)
CCR2
CX3CR1
TLR8
CD180
CD200R1
TLR7
TRPS1
CCR5
EHF
CD36
C3AR1
NFKB1
CLEC12A
IRF8
ZNF367
RUNX3
CNBP
SLC7A5
SLC2A1
ATF4

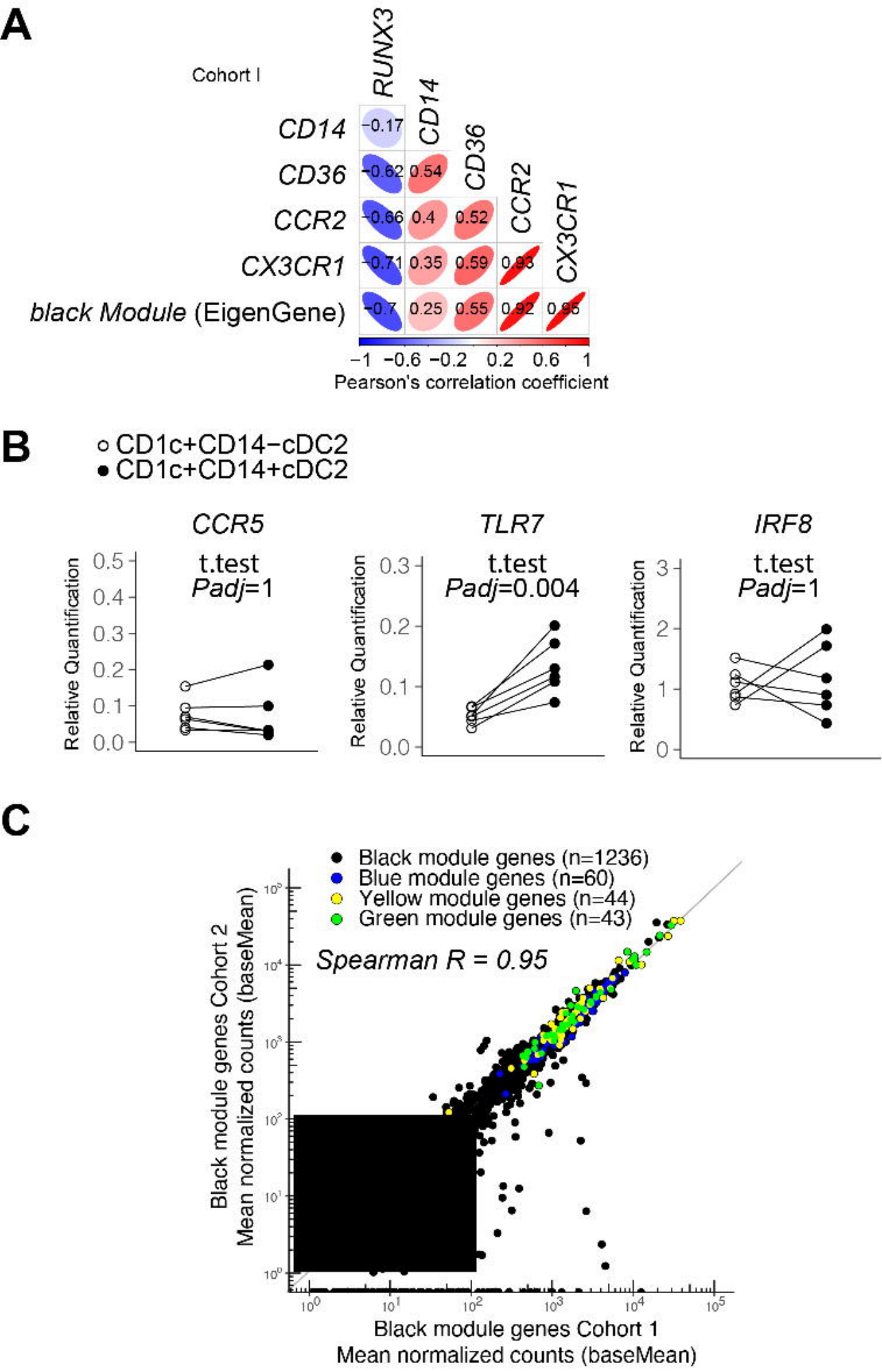
A
Cohort I
RUNX3
CD14
CD36
CCR2
CX3CR1
CD14
CD36
CCR2
CX3CR1
black Module (EigenGene)
−0.17
−0.62 0.54
−0.66 0.4 0.52
−0.71 0.35 0.59 0.93
−0.7 0.25 0.55 0.92 0.95
−1 −0.6 −0.2 0.2 0.6 1
Pearson's correlation coefficient
B
CD1c+CD14−cDC2
CD1c+CD14+cDC2
CCR5
t.test
Padj=1
TLR7
t.test
Padj=0.004
IRF8
t.test
Padj=1
Relative Quantification
C
Black module genes (n=1236)
Blue module genes (n=60)
Yellow module genes (n=44)
Green module genes (n=43)
Spearman R = 0.95
Black module genes Cohort 2
Mean normalized counts (baseMean)
Black module genes Cohort 1
Mean normalized counts (baseMean)

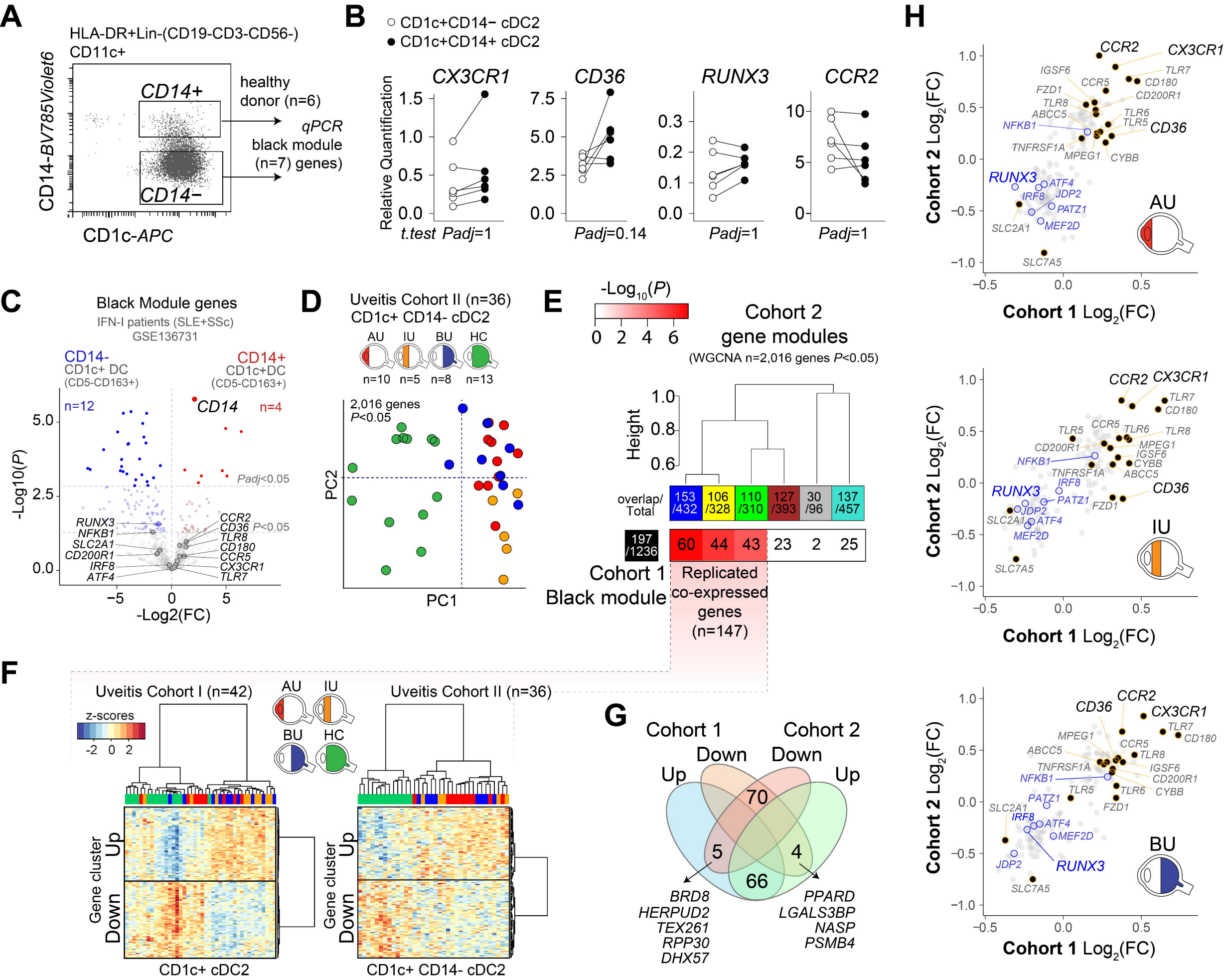
A
HLA-DR+Lin-(CD19-CD3-CD56-)
CD11c+
CD14+
CD14−
healthy donor (n=6)
qPCR black module (n=7) genes
CD14-BV785Violet6
CD1c-APC
B
CD1c+CD14− cDC2
CD1c+CD14+ cDC2
CX3CR1
CD36
RUNX3
CCR2
Relative Quantification
t.test Padj=1
Padj=0.14
Padj=1
Padj=1
C
Black Module genes
IFN-I patients (SLE+SSc)
GSE136731
CD14-
CD1c+ DC
(CD5-CD163+)
CD14+
CD1c+DC
(CD5-CD163+)
n=12
n=4
CD14
Padj<0.05
P<0.05
RUNX3
NFKB1
SLC2A1
CD200R1
IRF8
ATF4
CCR2
CD36
TLR8
CD180
CCR5
CX3CR1
TLR7
-Log10(P)
-Log2(FC)
D
Uveitis Cohort II (n=36)
CD1c+ CD14- cDC2
AU
IU
BU
HC
n=10
n=5
n=8
n=13
2,016 genes
P<0.05
PC2
PC1
E
-Log10(P)
Cohort 2
gene modules
(WGCNA n=2,016 genes P<0.05)
Height
overlap/ Total
153 /432
106 /328
110 /310
127 /393
30 /96
137 /457
197 /1236
60
44
43
23
2
25
Cohort 1
Black module
Replicated co-expressed genes (n=147)
H
CCR2
CX3CR1
IGSF6
TLR7
CCR5
CD180
FZD1
CD200R1
TLR8
ABCC5
TLR6
TLR5
NFKB1
CD36
TNFRSF1A
MPEG1
CYBB
RUNX3
ATF4
IRF8
JDP2
PATZ1
SLC2A1
MEF2D
SLC7A5
AU
IU
BU
Cohort 2 Log2(FC)
Cohort 1 Log2(FC)
F
Uveitis Cohort I (n=42)
Uveitis Cohort II (n=36)
z-scores
-2 0 2
Gene cluster
Up
Down
CD1c+ cDC2
CD1c+ CD14- cDC2
G
Cohort 1
Cohort 2
Up
Down
Down
Up
70
5
4
66
BRD8
HERPUD2
TEX261
RPP30
DHX57
PPARD
LGALS3BP
NASP
PSMB4

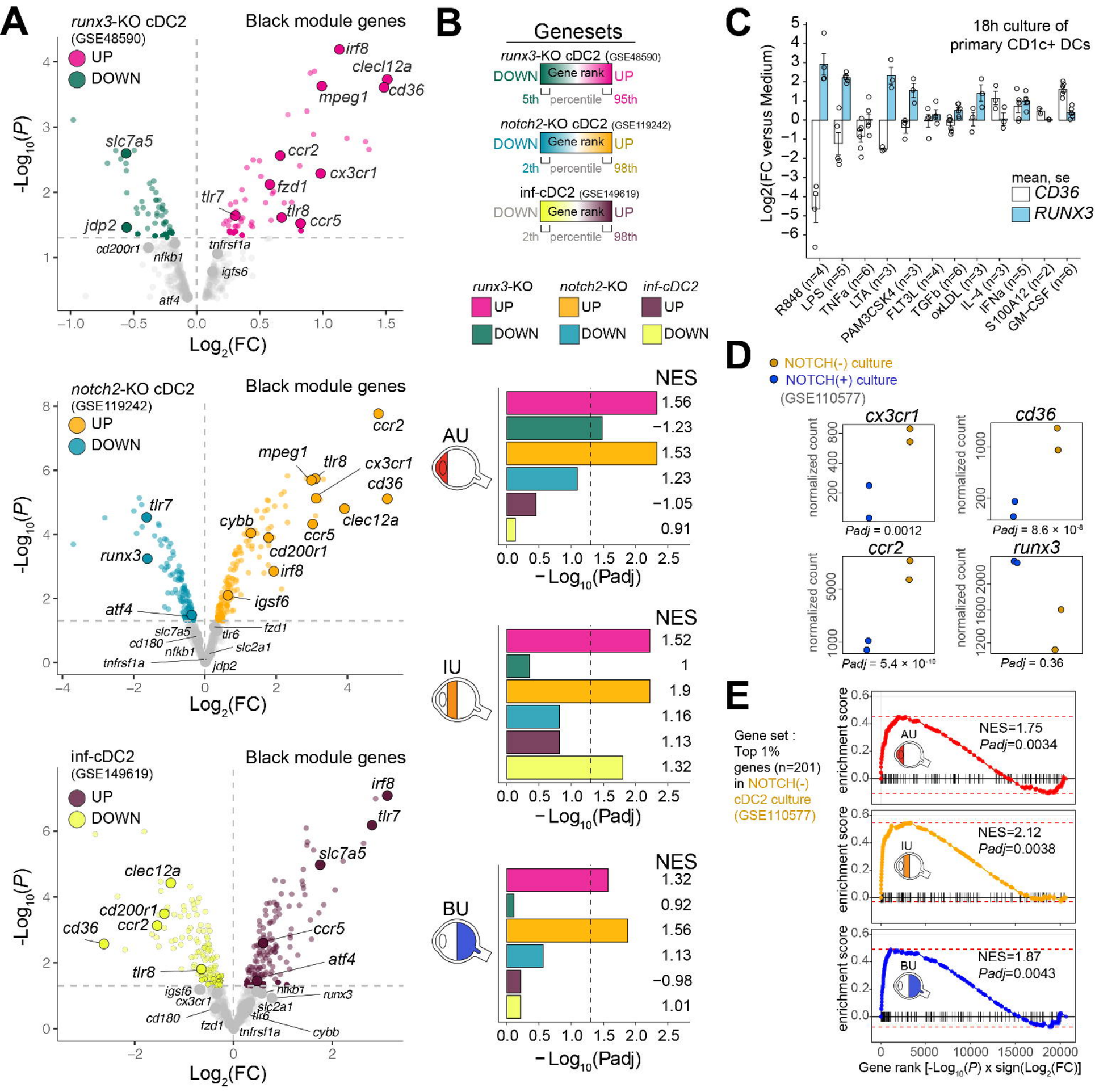
A
runx3-KO cDC2
(GSE48590)
UP
DOWN
Black module genes
irf8
clecl12a
cd36
mpeg1
slc7a5
ccr2
cx3cr1
fzd1
tlr7
tlr8
ccr5
jdp2
cd200r1
nfkb1
tnfrsf1a
igfs6
atf4
-Log10(P)
Log2(FC)
notch2-KO cDC2
(GSE119242)
UP
DOWN
Black module genes
ccr2
mpeg1
tlr8
cx3cr1
cd36
tlr7
cybb
clec12a
ccr5
runx3
cd200r1
irf8
igsf6
atf4
slc7a5
tlr6
fzd1
cd180
nfkb1
slc2a1
tnfrsf1a
jdp2
-Log10(P)
Log2(FC)
inf-cDC2
(GSE149619)
UP
DOWN
Black module genes
irf8
tlr7
slc7a5
clec12a
cd200r1
cd36
ccr2
ccr5
atf4
tlr8
igsf6
nfkb1
runx3
cx3cr1
slc2a1
cd180
tlr6
fzd1
tnfrsf1a
cybb
-Log10(P)
Log2(FC)
B
Genesets
runx3-KO cDC2 (GSE48590)
DOWN Gene rank UP
5th percentile 95th
notch2-KO cDC2 (GSE119242)
DOWN Gene rank UP
2th percentile 98th
inf-cDC2 (GSE149619)
DOWN Gene rank UP
2th percentile 98th
runx3-KO
UP
DOWN
notch2-KO
UP
DOWN
inf-cDC2
UP
DOWN
AU
NES
1.56
−1.23
1.53
1.23
−1.05
0.91
−Log10(Padj)
IU
NES
1.52
1
1.9
1.16
1.13
1.32
−Log10(Padj)
BU
NES
1.32
0.92
1.56
1.13
−0.98
1.01
−Log10(Padj)
C
18h culture of
primary CD1c+ DCs
Log2(FC versus Medium)
mean, se
CD36
RUNX3
R848 (n=4)
LPS (n=5)
TNFa (n=6)
LTA (n=3)
PAM3CSK4 (n=3)
FLT3L (n=4)
TGFb (n=6)
oxLDL (n=3)
IL-4 (n=3)
IFNa (n=5)
S100A12 (n=2)
GM-CSF (n=6)
D
NOTCH(-) culture
NOTCH(+) culture
(GSE110577)
cx3cr1
normalized count
Padj = 0.0012
cd36
normalized count
Padj = 8.6 × 10-8
ccr2
normalized count
Padj = 5.4 × 10-10
runx3
normalized count
Padj = 0.36
E
Gene set :
Top 1%
genes (n=201)
in NOTCH(-)
cDC2 culture
(GSE110577)
AU
NES=1.75
Padj=0.0034
IU
NES=2.12
Padj=0.0038
BU
NES=1.87
Padj=0.0043
enrichment score
Gene rank [-Log10(P) x sign(Log2(FC))]

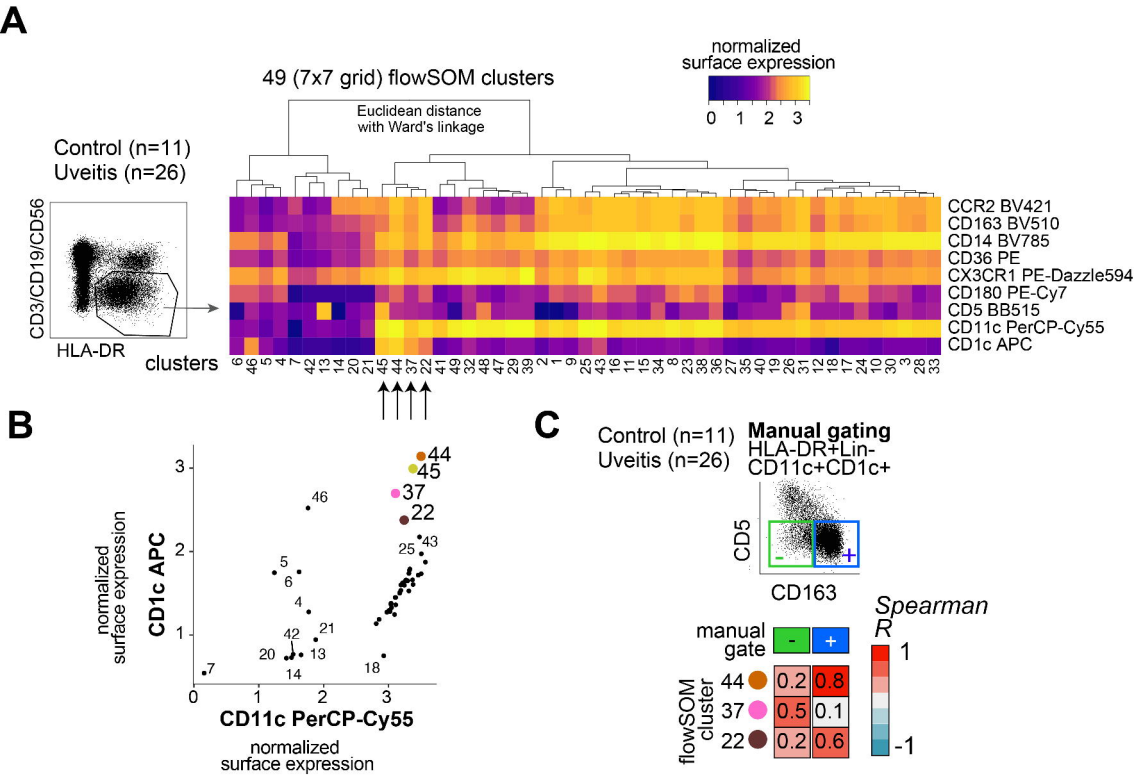
A
49 (7x7 grid) flowSOM clusters
Euclidean distance with Ward's linkage
normalized surface expression
0 1 2 3
Control (n=11)
Uveitis (n=26)
CD3/CD19/CD56
HLA-DR
clusters
CCR2 BV421
CD163 BV510
CD14 BV785
CD36 PE
CX3CR1 PE-Dazzle594
CD180 PE-Cy7
CD5 BB515
CD11c PerCP-Cy55
CD1c APC
B
CD1c APC
normalized surface expression
CD11c PerCP-Cy55
normalized surface expression
C
Control (n=11)
Uveitis (n=26)
Manual gating
HLA-DR+Lin-
CD11c+CD1c+
CD5
CD163
manual gate
flowSOM cluster
Spearman R
1
-1
44 0.2 0.8
37 0.5 0.1
22 0.2 0.6

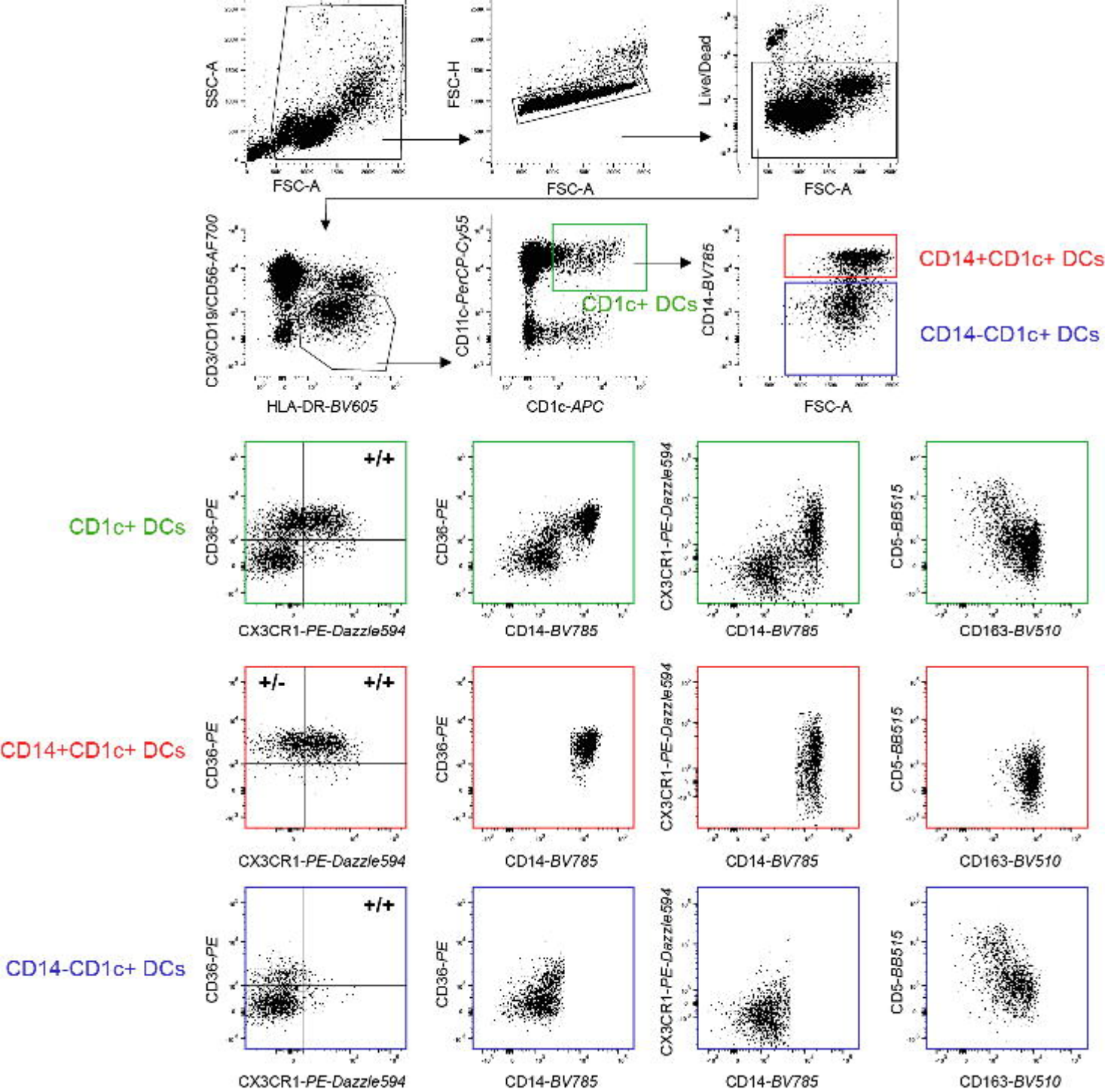
SSC-A
FSC-A
FSC-H
FSC-A
Live/Dead
FSC-A
CD3/CD19/CD56-AF700
HLA-DR-BV605
CD11c-PerCP-Cy55
CD1c-APC
CD1c+ DCs
CD14-BV785
FSC-A
CD14+CD1c+ DCs
CD14-CD1c+ DCs
CD1c+ DCs
+/+
CD36-PE
CX3CR1-PE-Dazzle594
CD36-PE
CD14-BV785
CX3CR1-PE-Dazzle594
CD14-BV785
CD5-BB515
CD163-BV510
CD14+CD1c+ DCs
+/-
+/+
CD36-PE
CX3CR1-PE-Dazzle594
CD36-PE
CD14-BV785
CX3CR1-PE-Dazzle594
CD14-BV785
CD5-BB515
CD163-BV510
CD14-CD1c+ DCs
+/+
CD36-PE
CX3CR1-PE-Dazzle594
CD36-PE
CD14-BV785
CX3CR1-PE-Dazzle594
CD14-BV785
CD5-BB515
CD163-BV510

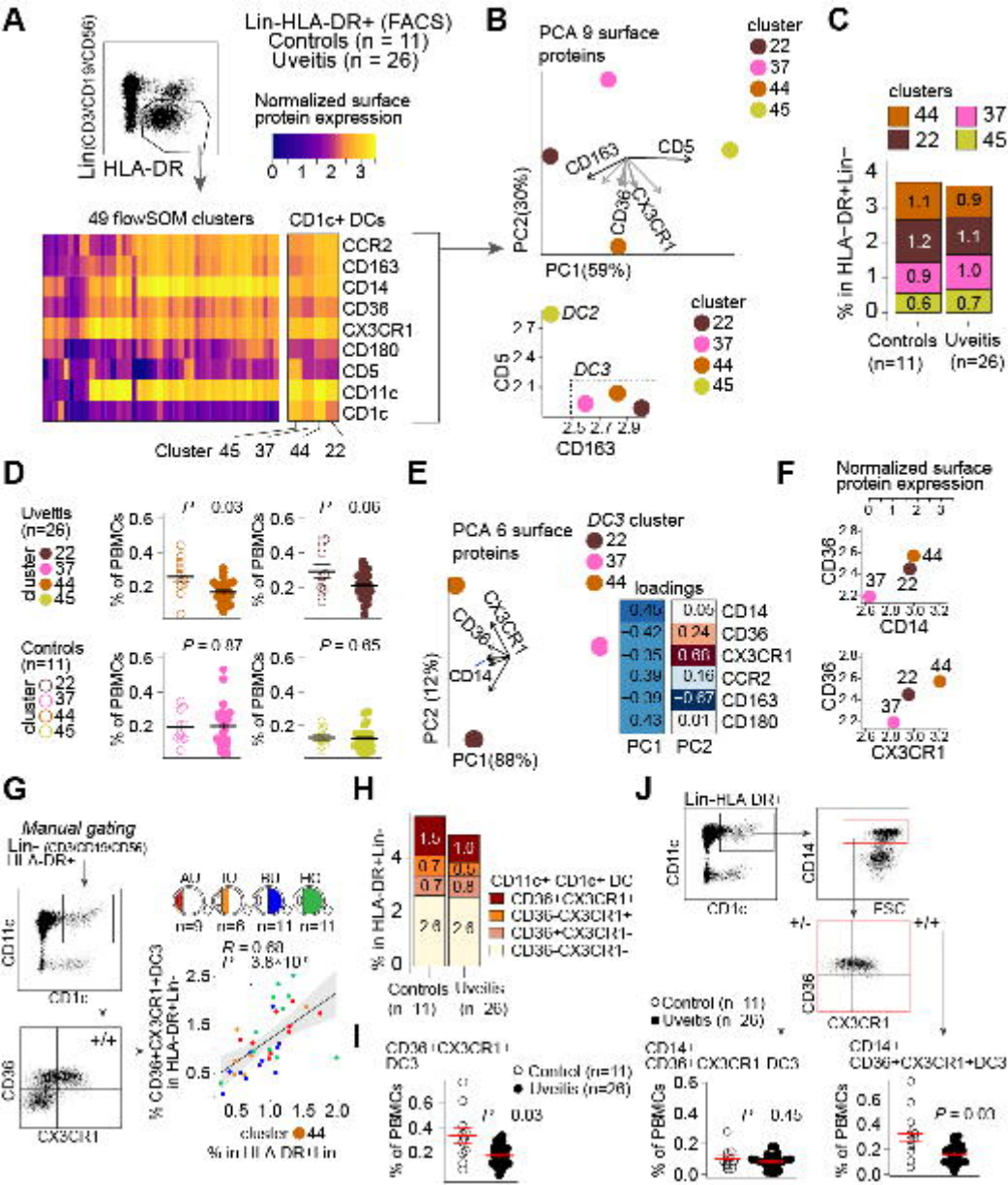
A
Lin-HLA-DR+ (FACS)
Controls (n = 11)
Uveitis (n = 26)
Lin(CD3/CD19/CD56)
HLA-DR
Normalized surface protein expression
0 1 2 3
49 flowSOM clusters
CD1c+ DCs
CCR2
CD163
CD14
CD36
CX3CR1
CD180
CD5
CD11c
CD1c
Cluster 45 37 44 22
B
PCA 9 surface proteins
cluster
22
37
44
45
CD163
CD5
CD36
CX3CR1
PC2(30%)
PC1(59%)
DC2
DC3
CD5
CD163
C
clusters
% in HLA-DR+Lin-
Controls (n=11)
Uveitis (n=26)
D
Uveitis (n=26)
Controls (n=11)
% of PBMCs
P = 0.03
P = 0.06
P = 0.07
P = 0.65
E
PCA 6 surface proteins
DC3 cluster
loadings
CD14
CD36
CX3CR1
CCR2
CD163
CD180
PC1
PC2
PC2 (12%)
PC1(88%)
F
Normalized surface protein expression
CD36
CD14
CX3CR1
G
Manual gating
Lin- (CD3/CD19/CD56)
HLA-DR+
CD11c
CD1c
CD36
CX3CR1
+/+
AU
IU
BU
HC
n=9
n=6
n=11
n=26
R = 0.60
P = 3.8×10⁻⁴
% CD36+CX3CR1+DC3 in HLA-DR+Lin-
cluster 44
% in HLA-DR+Lin-
H
% in HLA-DR+Lin-
CD11c+ CD1c+ DC
CD36+CX3CR1+
CD36+CX3CR1-
CD36-CX3CR1-
Controls (n=11)
Uveitis (n=26)
I
CD36+CX3CR1+ DC3
Control (n=11)
Uveitis (n=26)
% of PBMCs
P = 0.03
J
Lin-HLA-DR+
CD11c
CD1c
CD14
FSC
+/-
+/+
CD36
CX3CR1
Control (n=11)
Uveitis (n=26)
CD14+ CD36+CX3CR1+ DC3
P = 0.15
P = 0.03

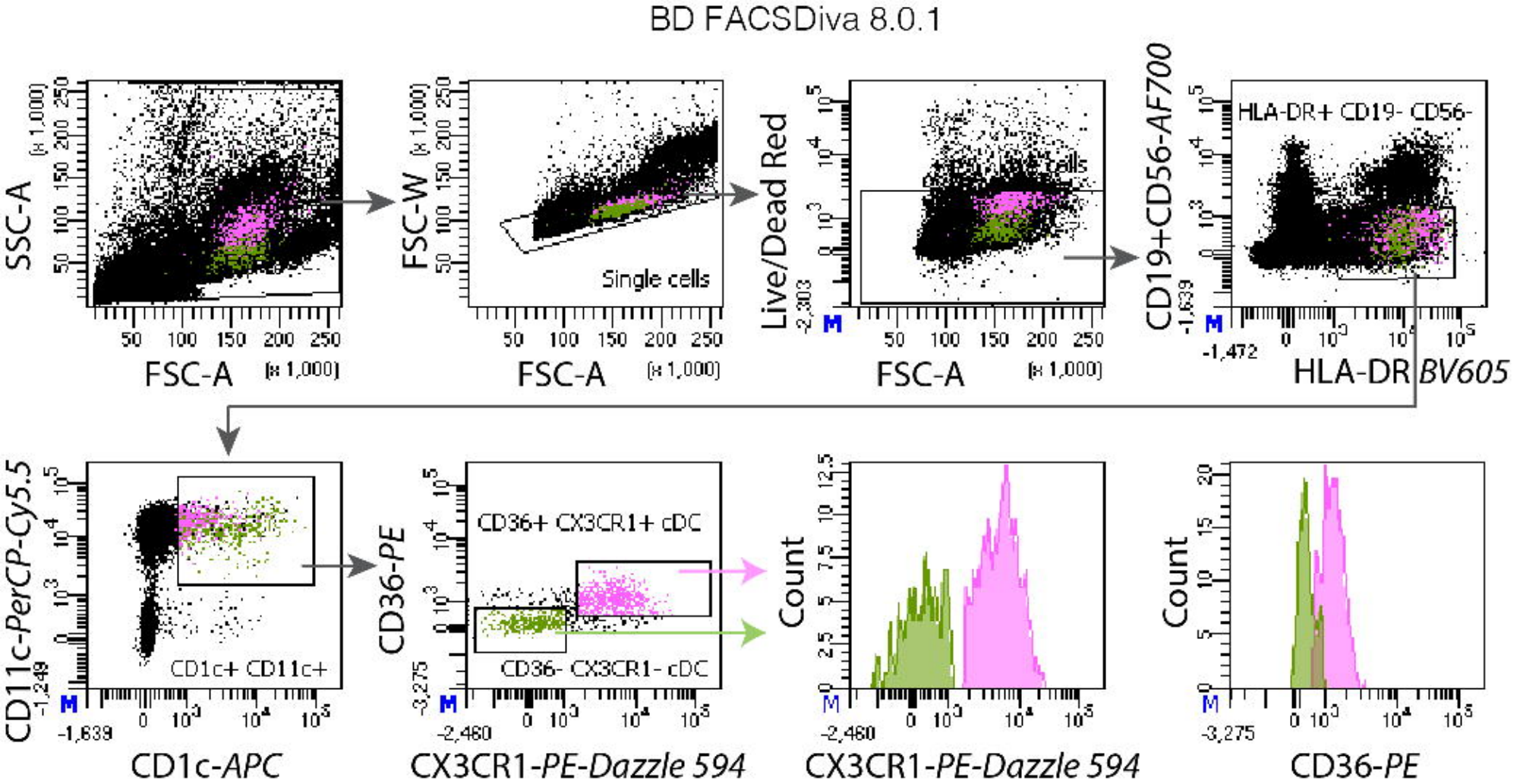

Tube: donor 1 Buffy

Population	#Events	%Parent	%Total
All Events	181,274	####	100.0
FCS/SSC	100,037	55.2	55.2
Single cells	94,165	94.1	51.9
Live cells	92,026	97.7	50.8
HLA-DR+ CD19- CD56-	20,907	22.7	11.5
CD1c+ CD11c+	1,135	5.4	0.6
CD36+ CX3CR1+ cDC	589	51.9	0.3
CD36- CX3CR1- cDC	345	30.4	0.2

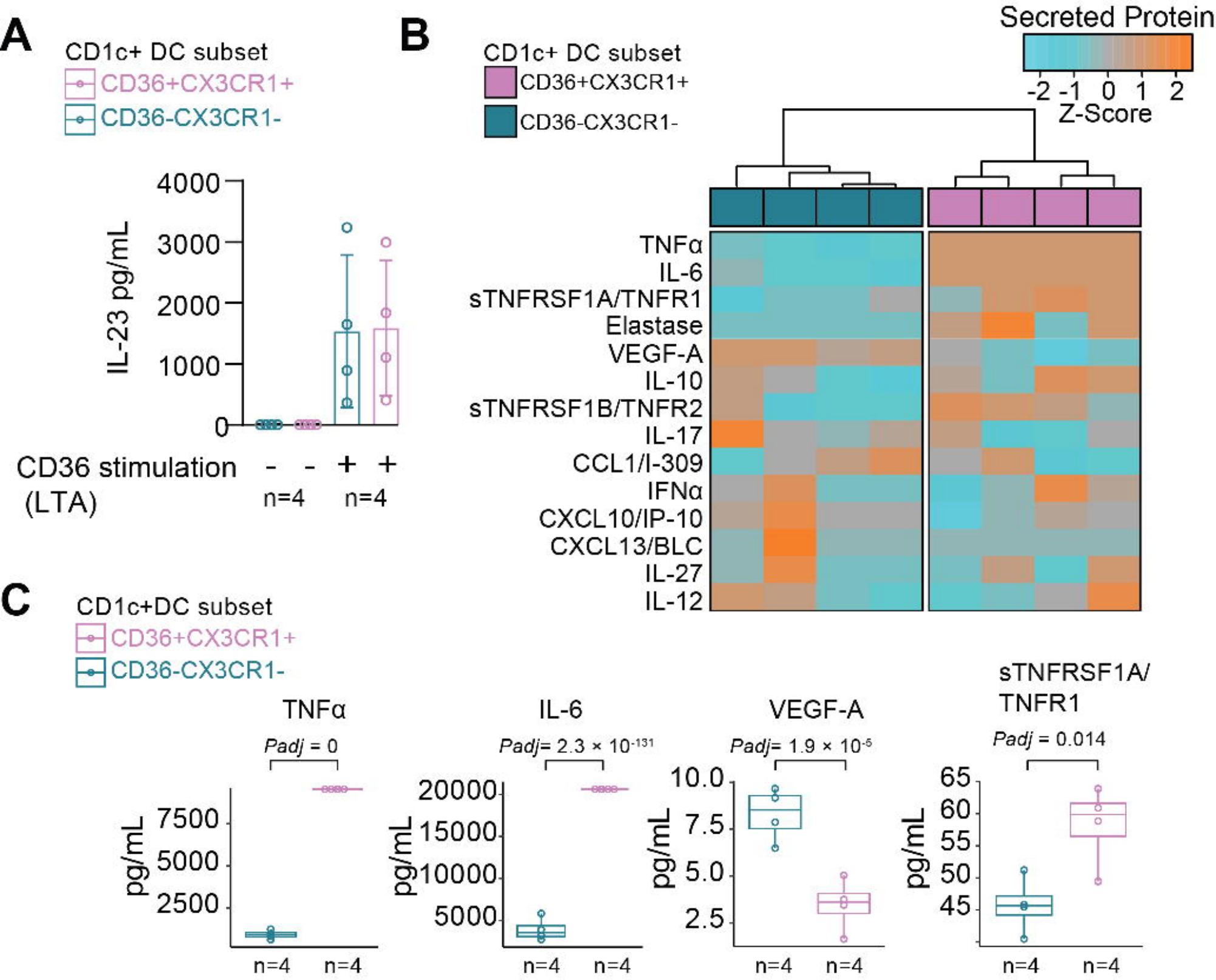
A
CD1c+ DC subset
CD36+CX3CR1+
CD36-CX3CR1-
IL-23 pg/mL
4000
3000
2000
1000
0
CD36 stimulation (LTA)
- - + +
n=4 n=4
B
CD1c+ DC subset
CD36+CX3CR1+
CD36-CX3CR1-
Secreted Protein
-2 -1 0 1 2
Z-Score
TNFα
IL-6
sTNFRSF1A/TNFR1
Elastase
VEGF-A
IL-10
sTNFRSF1B/TNFR2
IL-17
CCL1/I-309
IFNα
CXCL10/IP-10
CXCL13/BLC
IL-27
IL-12
C
CD1c+DC subset
CD36+CX3CR1+
CD36-CX3CR1-
TNFα
Padj = 0
IL-6
Padj= 2.3 × 10-131
VEGF-A
Padj= 1.9 × 10-5
sTNFRSF1A/ TNFR1
Padj = 0.014
pg/mL
n=4 n=4

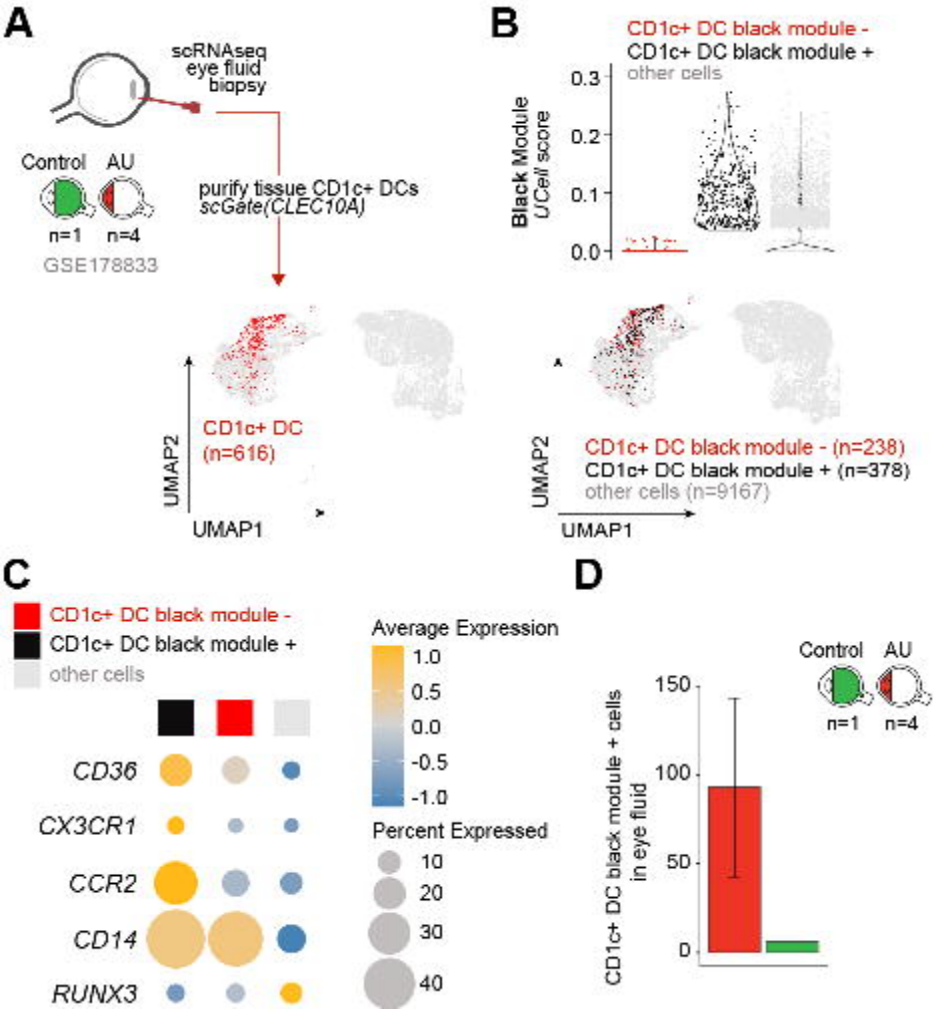
A
scRNAseq
eye fluid
biopsy
Control
AU
n=1
n=4
GSE178833
purify tissue CD1c+ DCs
scGate(CLEC10A)
CD1c+ DC
(n=616)
UMAP2
UMAP1
B
CD1c+ DC black module -
CD1c+ DC black module +
other cells
Black Module
UCell score
0.3
0.2
0.1
0.0
CD1c+ DC black module - (n=238)
CD1c+ DC black module + (n=378)
other cells (n=9167)
UMAP2
UMAP1
C
CD1c+ DC black module -
CD1c+ DC black module +
other cells
CD36
CX3CR1
CCR2
CD14
RUNX3
Average Expression
1.0
0.5
0.0
-0.5
-1.0
Percent Expressed
10
20
30
40
D
Control
AU
n=1
n=4
CD1c+ DC black module + cells
in eye fluid
150
100
50
0